

## AN EXTENDED FINITE ELEMENT METHOD FOR 2D EDGE ELEMENTS

FRANÇOIS LEFÈVRE, STEPHANIE LOHRENGEL, AND SERGE NICAISE

**Abstract.** A new eXtended Finite Element Method based on two-dimensional edge elements is presented and applied to solve the time-harmonic Maxwell equations in domains with cracks. Error analysis is performed and shows the method to be convergent with an order of at least  $\mathcal{O}(h^{1/2-\eta})$ . The implementation of the method is discussed and numerical tests illustrate its performance.

**Key words.** Maxwell's equations, domains with cracks, XFEM, singularities of solutions

### 1. Introduction

EXtended Finite Element Methods (XFEM) have gathered much interest in the domain of fracture mechanics in the last ten years since they are able to simulate the behavior of the displacement field in cracked regions using a mesh that is independent of the crack geometry. Hence, a single mesh can be used in the simulation of crack propagation, avoiding remeshing at each time step as well as reprojecting the solution on the updated mesh. The XFEM methodology was introduced by Moës *et al.* in 1999 [23]. Its main idea consists in enriching the basis of a standard Lagrange Finite Element Method by a step function along the crack in order to take into account the discontinuity of the displacement field across the crack. Moreover, the singular behavior of the solution near the crack tip is taken into account exactly by the addition of some singular functions, similar to the idea of the singular function method of Strang and Fix (see [30]). In the initial method of Moës *et al.*, only the nodes of the element containing the crack tip are provided with crack tip enrichment and the method is shown to converge with a rate of  $\mathcal{O}(\sqrt{h})$  as does a classical Finite Element Method in a cracked domain. To improve these results, several variants of the method have been developed. Béchet *et al.* [3] and Laborde *et al.* [20] introduce crack tip enrichment in a fixed area around the crack tip independent from the mesh size and get nearly optimal convergence rates. In [6, 8], a regular cut-off function with a mesh-independent support is used to localize the crack tip enrichment and a mathematical error analysis is performed. The XFEM methodology has been generalized to three-dimensional planar and non-planar cracks [32, 24, 15] as well as to new application fields as two-phase flows or fluid-structure interaction [9, 14]. To some extent, XFEM can be interpreted as a fictitious domain method as it has been pointed out in [17]. Indeed, both methods use meshes of a domain of simple geometry (like a rectangle or disk), and the shape of the physical domain  $\Omega$  is taken into account in the variational formulation and the discretization spaces. This can be done by multiplying the shape functions of the finite element space by some appropriated function depending on the geometry of  $\Omega$ : the characteristic function of  $\Omega$  in the fictitious domain approach (see e.g. [5, 17]), a step function of Heaviside-type in XFEM. Usually, fictitious domain methods are based on a mixed formulation involving a Lagrange multiplier in order

to deal with Dirichlet boundary conditions. In the original XFEM approach, the boundary condition is of Neumann-type and hence there is no need for a mixed formulation. We refer to [22, 31] for a generalization to Dirichlet-type conditions.

In this paper, we propose a new eXtended Finite Element Method based on two-dimensional edge elements that are commonly used in the discretization of the Maxwell equations (see [28] for the original paper by Nédélec and [25] for a general presentation in three dimensions). We focus on a simple model problem which describes the time-harmonic Maxwell equations in a translation invariant setting resulting in a two-dimensional problem. To our knowledge, it is the first time that an XFEM-type method is applied in the context of computational electromagnetism. Some fictitious domain methods for electromagnetic scattering problems have been proposed for example in [5, 12, 13], but in general the obstacle is given by some regular domain. The simulation of the electromagnetic field in the presence of cracks is important for instance in electromagnetic testing which is a special technique of non destructive testing in order to detect defects inside a conducting test object as metallic tubes or aircraft fuselage. The discretization of the electromagnetic field in the neighborhood of geometric singularities is quite difficult since the singular behavior is much stronger than in fracture mechanics: near a crack tip, the asymptotic behavior is as  $r^{-1/2}$  for the electromagnetic field compared to  $r^{1/2}$  for the displacement field in linear elasticity. On a geometry-dependent mesh, edge finite elements can handle these singularities provided the mesh is sufficiently refined near the singular points of the geometry [29]. In [4], a singular field method based on Lagrange Finite Elements has been presented for the time-harmonic Maxwell equations for different settings of the problem including regions with screens. Singularities of the electromagnetic field have been studied for polygons and Lipschitz polyhedra in [11, 27] and the analysis carries over to cracked domains.

As for the nodal XFEM, our eXtended Finite Element Method based on edge elements takes into account the *a priori* knowledge on the exact solution. On the one hand, the standard discretization space of edge elements is enriched by some basis functions multiplied with a step function of Heaviside-type in order to enable the tangential component of the approximate solution field to be discontinuous across the crack. On the other hand, appropriated singular fields are added to the discretization space in order to take into account the singular behavior near the crack tip. These singular fields are derived from the singular functions associated with the scalar Laplace operator.

The paper is organized as follows: in §2, we define the variational setting of the model problem and introduce the singular functions that describe the behavior of the solution field near the crack tip. We prove the decomposition of the solution into a regular and a singular part and give the global regularity of the regular part. In §3, we define the discretization space for the XFEM based on two dimensional edge elements and prove that the discretization is conforming in  $\mathcal{H}(\text{curl}, \Omega)$ . Section 4 is devoted to the analysis of the XFEM interpolation error which yields a convergence rate of the method of at least  $\mathcal{O}(h^{1/2-\eta})$  due to Céa's lemma. In §5, we discuss the implementation of the method and give a series of numerical results illustrating the theory and the performance of the method. Finally, we postpone in Appendix A some technical results concerning a vector extension operator involved in the error analysis in §4.

## 2. The model problem

In this paper, we focus on a simple model problem. We consider the time-harmonic Maxwell equations in a two dimensional cracked domain  $\Omega$ . Eliminating

the magnetic field yields

$$(1) \quad \mathbf{curl} \mu_r^{-1} \mathbf{curl} \mathbf{E} - \kappa^2 \varepsilon_r \mathbf{E} = \mathbf{f} \quad \text{in } \Omega$$

where  $\mathbf{E}$  is the electric field and  $\mathbf{f}$  is the applied current density. The notations  $\mathbf{curl}$  and  $\mathbf{curl}$  distinguish between the scalar and vector curl operators,

$$\mathbf{curl} \mathbf{E} = \frac{\partial E_2}{\partial x_1} - \frac{\partial E_1}{\partial x_2} \quad \text{and} \quad \mathbf{curl} \varphi = \left( \frac{\partial \varphi}{\partial x_2}, -\frac{\partial \varphi}{\partial x_1} \right)^t.$$

In (1),  $\kappa = \omega \sqrt{\varepsilon_0 \mu_0}$  for a given frequency  $\omega > 0$  where  $\mu_0 > 0$  and  $\varepsilon_0 > 0$  are respectively the magnetic permeability and electric permittivity in free space. We consider a homogeneous conducting material with relative permeability  $\mu_r$  and permittivity  $\varepsilon_r$  defined by

$$\mu_r = \frac{\mu}{\mu_0} \quad \text{and} \quad \varepsilon_r = \frac{1}{\varepsilon_0} \left( \varepsilon + \frac{i\sigma}{\omega} \right)$$

where  $\mu > 0$ ,  $\varepsilon > 0$  and  $\sigma > 0$  are, respectively, the magnetic permeability, the electric permittivity and the electric conductivity of the material.

In order to make precise the geometric setting of the problem, let  $Q \subset \mathbb{R}^2$  be an open convex polygon and  $\Gamma = \partial Q$  its boundary. Let  $\Sigma = \{sx^* + (1-s)x_\Gamma; s \in [0, 1]\}$  be a closed segment in  $\overline{Q}$ , called the crack. We assume the crack to be emerging, meaning that the crack tip  $x^*$  belongs to  $Q$  whereas  $x_\Gamma \in \Gamma$  is a point of the boundary (see Figure 1).

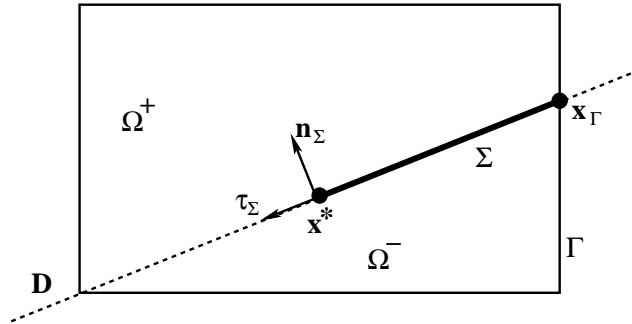


FIGURE 1. Model domain with a crack.

Let  $\tau_\Sigma$  be the unit tangent vector of  $\Sigma$  given by

$$\tau_\Sigma = \frac{\overrightarrow{x_\Gamma x^*}}{\|\overrightarrow{x_\Gamma x^*}\|}.$$

Let  $\mathbf{n}_\Sigma$  be the unit normal vector on  $\Sigma$  such that the orientation of the system  $(\mathbf{n}_\Sigma, \tau_\Sigma)$  is direct. The crack  $\Sigma$  is a subset of the straight line

$$\mathcal{D} = \{ \mathbf{x} \in \mathbb{R}^2 \mid (\mathbf{x} - \mathbf{x}^*) \cdot \mathbf{n}_\Sigma = 0 \}.$$

Let  $\Omega = Q \setminus \Sigma$  be the domain outside the crack. Finally, let  $(\Omega^+, \Omega^-)$  be a partition of  $\Omega$  such that for any  $\mathbf{x} \in \Omega$ ,

$$\begin{aligned} \mathbf{x} &\in \Omega^+ \quad \text{if} \quad (\mathbf{x} - \mathbf{x}^*) \cdot \mathbf{n}_\Sigma > 0 \\ \mathbf{x} &\in \Omega^- \quad \text{if} \quad (\mathbf{x} - \mathbf{x}^*) \cdot \mathbf{n}_\Sigma < 0. \end{aligned}$$

The partial differential equation (1) is completed with the following two boundary conditions on  $\Gamma$  and  $\Sigma$ , respectively,

$$(2) \quad \mathbf{E} \times \mathbf{n} = 0 \text{ on } \Gamma$$

$$(3) \quad \mu_r^{-1} \operatorname{curl} \mathbf{E} \times \mathbf{n}_\Sigma = 0 \text{ on } \Sigma,$$

where  $\mathbf{E} \times \mathbf{n} = E_1 n_2 - E_2 n_1$  in two dimensions. The perfect conducting boundary condition on  $\Gamma$  has been chosen for the sake of simplicity of the presentation and could be replaced by an impedance-like condition. On  $\Sigma$ , the condition is of Neumann-type, allowing the tangential component of the electric field to be discontinuous across the crack.

Let us introduce the functional space of vector fields with finite electromagnetic energy,

$$\mathcal{H}(\operatorname{curl}; \Omega) = \{ \mathbf{v} \in L^2(\Omega)^2 \mid \operatorname{curl} \mathbf{v} \in L^2(\Omega) \},$$

equipped with the norm

$$\| \mathbf{v} \|_{\mathcal{H}(\operatorname{curl}; \Omega)} = \left( \| \mathbf{v} \|_{0, \Omega}^2 + \| \operatorname{curl} \mathbf{v} \|_{0, \Omega}^2 \right)^{\frac{1}{2}}.$$

Here  $\| \cdot \|_{0, \Omega}$  denotes without distinction the  $L^2$ -norm for vector fields and scalar functions. The variational formulation of problem (1)–(2)–(3) involves the space

$$\mathcal{H}_{0, \Gamma}(\operatorname{curl}; \Omega) = \{ \mathbf{v} \in \mathcal{H}(\operatorname{curl}; \Omega) \mid \mathbf{v} \times \mathbf{n} = 0 \text{ on } \Gamma \}$$

and reads as follows

$$(P) \quad \begin{cases} \text{Find } \mathbf{u} \in \mathcal{H}_{0, \Gamma}(\operatorname{curl}; \Omega) \text{ such that} \\ (\mu_r^{-1} \operatorname{curl} \mathbf{u}, \operatorname{curl} \mathbf{v}) - \kappa^2 (\varepsilon_r \mathbf{u}, \mathbf{v}) = (\mathbf{f}, \mathbf{v}) \quad \forall \mathbf{v} \in \mathcal{H}_{0, \Gamma}(\operatorname{curl}; \Omega) \end{cases}$$

where  $\mathbf{f} \in L^2(Q)^2$  is such that  $\operatorname{div} \mathbf{f} \in L^2(Q)$ .

Notice that the sesquilinear form

$$a(\mathbf{u}, \mathbf{v}) = (\mu_r^{-1} \operatorname{curl} \mathbf{u}, \operatorname{curl} \mathbf{v}) - \kappa^2 (\varepsilon_r \mathbf{u}, \mathbf{v})$$

is coercive on  $\mathcal{H}_{0, \Gamma}(\operatorname{curl}; \Omega)$  since  $\sigma > 0$ . Indeed, the assumption on  $\sigma$  assures that there is  $\theta \in ]\frac{\pi}{2}, \pi[$  such that  $-\kappa^2 \varepsilon_r = |\kappa^2 \varepsilon_r| e^{-i\theta}$ . Therefore,

$$\Re \left( e^{i\frac{\theta}{2}} a(\mathbf{u}, \mathbf{u}) \right) \geq \cos\left(\frac{\theta}{2}\right) \min(\mu_r^{-1}, |\kappa^2 \varepsilon_r|) \| \mathbf{u} \|_{\mathcal{H}(\operatorname{curl}; \Omega)}^2$$

which yields the coercivity (see [18]). Thus, problem (P) has a unique solution for any  $\omega > 0$  owing to the Lax-Milgram lemma.

Actually, the solution of problem (P) can be shown to belong to the vector space

$$(4) \quad \mathcal{H}_{0, \Sigma}(\operatorname{div}; \Omega) = \{ \mathbf{v} \in L^2(\Omega)^2 \mid \operatorname{div} \mathbf{v} \in L^2(\Omega) \text{ and } \mathbf{v} \cdot \mathbf{n}_\Sigma = 0 \text{ on } \Sigma \}.$$

**Proposition 1.** *Assume that  $\mathbf{f} \in L^2(Q)^2$  and  $\operatorname{div} \mathbf{f} \in L^2(Q)$ . Then the solution  $\mathbf{u}$  of (P) belongs to  $\mathcal{H}_{0, \Sigma}(\operatorname{div}; \Omega)$ .*

*Proof.* Let  $\mathbf{u} \in \mathcal{H}_{0, \Gamma}(\operatorname{curl}; \Omega)$  be the solution of (P). Taking  $\mathbf{v} = \operatorname{grad} \varphi$  with  $\varphi \in H_0^1(\Omega)$  in the variational formulation yields  $\operatorname{div} \mathbf{u} = -(\kappa^2 \varepsilon_r)^{-1} \operatorname{div} \mathbf{f}$  in  $\Omega$ .

Next, let  $\varphi \in H_0^1(Q)$ . Then  $\mathbf{v} = \operatorname{grad} \varphi$  belongs to  $\mathcal{H}_{0, \Gamma}(\operatorname{curl}; \Omega)$  and is an admissible test field in (P). We thus have

$$-\kappa^2 (\varepsilon_r \mathbf{u}, \operatorname{grad} \varphi) = -(\operatorname{div} \mathbf{f}, \varphi)$$

according to the assumption on  $\mathbf{f}$ . Now, partial integration in the integrals over  $\Omega^+$  and  $\Omega^-$  on the left hand side yields

$$(5) \quad \int_{\partial\Omega^+} \mathbf{u} \cdot \mathbf{n} \varphi \, ds + \int_{\partial\Omega^-} \mathbf{u} \cdot \mathbf{n} \varphi \, ds = 0,$$

since  $\kappa^2 \varepsilon_r \operatorname{div} \mathbf{u} = -\operatorname{div} \mathbf{f}$  in  $\Omega^+$  and  $\Omega^-$ . (5) reduces to

$$\int_{D \cap Q} [\mathbf{u} \cdot \mathbf{n}_\Sigma] \varphi \, ds = 0$$

since  $\varphi$  vanishes on the boundary of  $Q$ . Here  $[\mathbf{u} \cdot \mathbf{n}_\Sigma]$  denotes the jump of the normal component of  $\mathbf{u}$  across the straight line  $D$  (see Figure 1). We thus get  $[\mathbf{u} \cdot \mathbf{n}_\Sigma] = 0$  in  $H_{00}^{-1/2}(D \cap Q)$  where  $H_{00}^{-1/2}(D \cap Q)$  denotes the dual of the space  $\tilde{H}^{1/2}(D \cap Q)$  of all functions  $\psi$  defined on  $D \cap Q$  such that the extension of  $\psi$  by zero outside  $D \cap Q$  belongs to  $H^{1/2}(D)$  (see [16] for the definition of the space  $\tilde{H}^{1/2}(D \cap \Omega)$  and its dual).

Finally, let  $\varphi \in H^1(\Omega)$  such that  $\varphi = 0$  on  $\Gamma$ . The jump of  $\varphi$  across  $D$  vanishes on  $(D \cap Q) \setminus \Sigma$  and  $[\varphi]_\Sigma$  belongs to  $\tilde{H}^{1/2}(\Sigma)$ . Again,  $\mathbf{v} = \operatorname{grad} \varphi$  can be taken as a test field in the variational formulation and we get

$$\int_{\Sigma} \mathbf{u} \cdot \mathbf{n}_\Sigma [\varphi]_\Sigma \, ds = 0$$

which proves that  $\mathbf{u} \cdot \mathbf{n}_\Sigma = 0$  in  $H_{00}^{-1/2}(\Sigma)$ . □

We now describe the singular functions associated with Problem  $(\mathcal{P})$  and the geometry described by Figure 1. Let  $\omega^\pm > 0$  be the opening angle between the crack  $\Sigma$  and  $\Gamma \cap \overline{\Omega^\pm}$ . Notice that  $\omega^+ + \omega^- \leq \pi$  since  $Q$  is assumed to be convex, and  $\omega^+ + \omega^- = \pi$  if  $x_\Gamma$  is not a vertex of  $Q$ . Near  $x_\Gamma$ , the asymptotic behavior of the electric field is derived from the singular functions of the scalar Laplace operator with mixed Dirichlet and Neumann boundary conditions (see [21]).

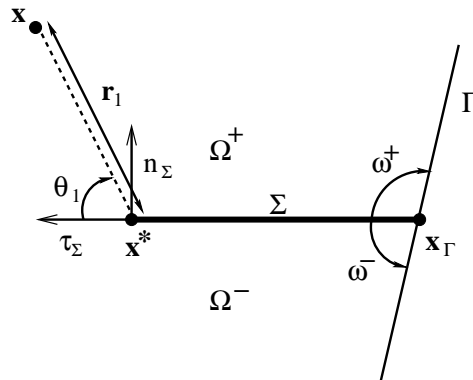


FIGURE 2. Local polar coordinates with respect to the crack tips.

Let  $(r_1, \theta_1)$  (resp.  $(r_2, \theta_2)$ ) denote the local polar coordinates with respect to  $x^*$  (resp.  $x_\Gamma$ ) according to Figure 2. The following singular function is associated with the crack tip  $x^*$ ,

$$S_1(r_1, \theta_1) = r_1^{1/2} \sin\left(\frac{\theta_1}{2}\right).$$

If  $\omega^+ > \frac{\pi}{2}$ , we define the singular function associated with  $x_\Gamma$  by

$$S_2(r_2, \theta_2) = \begin{cases} r_2^{\lambda^+} \sin(\lambda^+ \theta_2) & \text{in } \Omega^+, \\ 0 & \text{in } \Omega^-, \end{cases}$$

whereas

$$S_2(r_2, \theta_2) = \begin{cases} 0 & \text{in } \Omega^+, \\ r_2^{\lambda^-} \sin(\lambda^- \theta_2) & \text{in } \Omega^-. \end{cases}$$

if  $\omega^- > \frac{\pi}{2}$ . The singular exponent of  $S_2$  is given by  $\lambda^\pm = \frac{\pi}{2\omega^\pm}$ . Notice that  $S_\alpha \in H^1(\Omega)$  for  $\alpha \in \{1, 2\}$ , but  $S_\alpha \notin H^2(\Omega)$ . If neither  $\omega^+ > \frac{\pi}{2}$  nor  $\omega^- > \frac{\pi}{2}$ , no singular behavior is observed near  $x_\Gamma$  and the function  $S_2$  does not have to be considered. In the sequel, let  $\mathcal{I}$  be the index set for the singular functions, i.e.  $\mathcal{I} = \{1, 2\}$  or  $\mathcal{I} = \{1\}$ . Finally, let  $\eta_1$  (resp.  $\eta_2$ ) be a cut-off function in  $W^{2,\infty}(Q)$  with respect to  $x^*$  (resp.  $x_\Gamma$ ) such that  $\text{supp}(\eta_1) \cap \text{supp}(\eta_2) = \emptyset$ .

The following theorem yields the decomposition of the vector space involved in  $(\mathcal{P})$  into a regular part and a singular part deriving from a scalar potential.

**Theorem 1.** *Let  $\mathbf{V} = \mathcal{H}_{0,\Gamma}(\text{curl}; \Omega) \cap \mathcal{H}_{0,\Sigma}(\text{div}; \Omega)$ . The following direct decomposition of  $\mathbf{V}$  holds true.*

$$\mathbf{V} = (H^1(\Omega)^2 \cap \mathbf{V}) \oplus \text{Vect}(\text{grad}(\eta_\alpha S_\alpha) | \alpha \in \mathcal{I})$$

*Proof.* For the analysis near the crack tip, we refer to Theorem 1.1 of [11] where domains with cracks are allowed (see also [27]). The analysis near  $x_\Gamma$  is performed separately in  $\Omega^+$  and  $\Omega^-$ , and the decomposition follows from the results in [21].  $\square$

The next theorem states precisely the regularity of the solution of problem  $(\mathcal{P})$  which belongs to  $\mathcal{H}_{0,\Gamma}(\text{curl}; \Omega) \cap \mathcal{H}_{0,\Sigma}(\text{div}; \Omega)$  according to Proposition 1.

**Theorem 2.** *Let  $\mathbf{f} \in L^2(Q)^2$  such that  $\text{div } \mathbf{f} \in L^2(Q)$  and let  $\mathbf{u} \in \mathcal{H}_{0,\Gamma}(\text{curl}; \Omega)$  be the unique solution of  $(\mathcal{P})$ . Then for any  $\eta \in ]0, 1/2]$  we have*

$$(6) \quad \mathbf{u} = \mathbf{u}_r + \text{grad } \Phi,$$

where  $\mathbf{u}_r$  belongs to  $H^{3/2-\eta}(\Omega)^2$  and  $\Phi \in H^1_{0,\Gamma}(\Omega)$  is the variational solution of the following Poisson equation with mixed boundary conditions

$$\begin{aligned} -\Delta \Phi &= g && \text{in } \Omega \\ \Phi &= 0 && \text{on } \Gamma \\ \partial_n \Phi &= 0 && \text{on } \Sigma \end{aligned}$$

where  $g \in H^{1/2-\eta}(\Omega)$ . Moreover,

$$\|\mathbf{u}_r\|_{3/2-\eta,\Omega} + \|\Phi\|_{1,\Omega} + \|\Delta \Phi\|_{1/2-\eta,\Omega} \lesssim \|\mathbf{f}\|_{0,\Omega}.$$

We refer to Theorem 3.4 of [11] for the proof.

**Corollary 1.** *Under the assumptions of theorem 2, the solution  $\mathbf{u}$  of problem  $(\mathcal{P})$  satisfies  $\text{curl } \mathbf{u} \in H^1(\Omega)$ .*

*Proof.* The solution  $\mathbf{u}$  of problem  $(\mathcal{P})$  satisfies the partial differential equation

$$\mathbf{curl } \mu_r^{-1} \text{curl } \mathbf{u} - \kappa^2 \varepsilon_r \mathbf{u} = \mathbf{f}$$

where  $\mathbf{curl } \varphi = (\partial_2 \varphi, -\partial_1 \varphi)^t$  for any scalar function  $\varphi$ . Hence,  $\mathbf{curl } \mu_r^{-1} \text{curl } \mathbf{u}$  belongs to  $L^2(\Omega)^2$  which implies that  $\text{curl } \mathbf{u} \in H^1(\Omega)$  since  $\mu_r$  is constant on  $\Omega$ .  $\square$

The following embedding theorem follows from Theorem 1

**Theorem 3.** *The embedding  $\mathcal{H}_{0,\Gamma}(\text{curl}; \Omega) \cap \mathcal{H}_{0,\Sigma}(\text{div}; \Omega) \hookrightarrow L^2(\Omega)^2$  is compact.*

*Proof.* Let  $\mathbf{V} = \mathcal{H}_{0,\Gamma}(\text{curl}; \Omega) \cap \mathcal{H}_{0,\Sigma}(\text{div}; \Omega)$ . According to Theorem 1, the complement of  $H^1(\Omega)^2 \cap \mathbf{V}$  in  $\mathbf{V}$  is finite-dimensional, and the result follows from the compact embedding of  $H^1(\Omega)$  into  $L^2(\Omega)$ .  $\square$

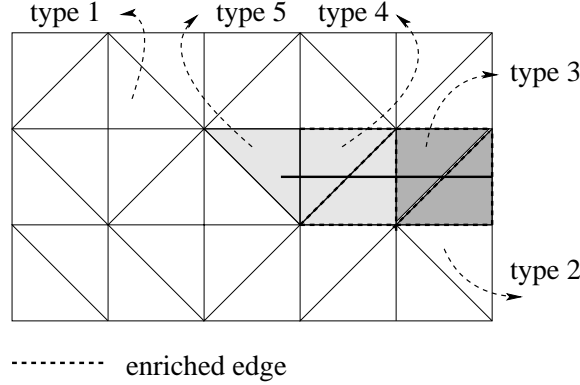


FIGURE 3. Edge enrichment.

### 3. Discretization by XFEM-edge elements

In the sequel, let  $\mathcal{T}_h$  be a triangulation of the (non-cracked) domain  $\bar{Q}$ . We recall that the classical edge elements of lowest order are defined by

$$\mathbf{X}_h^{\text{FE}} = \{ \mathbf{v}_h \in \mathcal{H}(\text{curl}; \Omega) \mid \mathbf{v}_h|_K \in \mathcal{R}_K \forall K \in \mathcal{T}_h \}$$

where

$$\mathcal{R}_K = \left\{ \mathbf{p} \in \mathbb{P}_1(K)^2 \mid \exists \mathbf{a} \in \mathbb{R}^2, b \in \mathbb{R}, \mathbf{p}(\mathbf{x}) = \mathbf{a} + b \begin{pmatrix} x_2 \\ -x_1 \end{pmatrix} \right\}.$$

Let  $\mathcal{E}$  denote the set of edges of the mesh  $\mathcal{T}_h$ . With each edge  $e$ , we associate the linear form

$$l_e(\mathbf{v}) = \int_e \gamma_e \mathbf{v} \cdot \mathbf{t}_e ds$$

where  $\mathbf{t}_e$  is the unit tangent vector of  $e$ . It is worth noticing that the definition of  $l_e(\cdot)$  depends on the orientation of the edge  $e$  which is fixed once and for all.  $l_e(\mathbf{v})$  is well defined for any vector field  $\mathbf{v}$  such that  $\gamma_e \mathbf{v} \in L^1(e)^2$ , where  $\gamma_e$  is the trace operator on the edge  $e$ . It follows from the properties of the elements in  $\mathbf{X}_h^{\text{FE}}$  that for a given edge  $e$ , there is a unique element  $\mathbf{w}_e \in \mathbf{X}_h^{\text{FE}}$  satisfying

$$l_{e'}(\mathbf{w}_e) = \delta_{ee'} \quad \forall e' \in \mathcal{E}.$$

The family  $(\mathbf{w}_e)_{e \in \mathcal{E}}$  is a basis of  $\mathbf{X}_h^{\text{FE}}$  and we have

$$\text{supp}(\mathbf{w}_e) = \bigcup \{ K \in \mathcal{T}_h \mid e \text{ is an edge of } K \}.$$

For any sufficiently smooth vector field  $\mathbf{v}$  defined on  $\Omega$ , the global interpolant in  $\mathbf{X}_h^{\text{FE}}$  is defined by

$$(7) \quad \mathbf{r}_h^{\text{FE}} \mathbf{v} = \sum_{e \in \mathcal{E}} l_e(\mathbf{v}) \mathbf{w}_e$$

and satisfies  $l_e(\mathbf{v} - \mathbf{r}_h^{\text{FE}} \mathbf{v}) = 0$  for any edge  $e \in \mathcal{E}$ . The local interpolant in  $\mathcal{R}_K$  is defined by restriction on  $K$ ,  $\mathbf{r}_K^{\text{FE}} \mathbf{v} = (\mathbf{r}_h^{\text{FE}} \mathbf{v})|_K$ .

Following the idea of the nodal XFEM, we introduce the set  $\mathcal{E}_H$  of enriched edges:  $e \in \mathcal{E}_H$  if the support of the corresponding basis function  $\mathbf{w}_e$  is cut by the crack into two disjoint parts of non-vanishing measure (see Figure 3).

We introduce different types of triangles taking into account the different enrichment strategies. For any triangle  $K \in \mathcal{T}_h$ , we denote by  $\mathcal{E}_K$  the set of its edges. We introduce the following subsets of  $\mathcal{T}_h$ :

$$\begin{aligned} \mathcal{K}_0 &= \{K \in \mathcal{T}_h \mid \text{card}(\mathcal{E}_K \cap \mathcal{E}_H) = 0 \text{ or } 1 \text{ and } x^* \notin \overline{K}\} \\ \mathcal{K}_H &= \{K \in \mathcal{T}_h \mid \text{card}(\mathcal{E}_K \cap \mathcal{E}_H) = 3\} \\ \mathcal{K}^* &= \{K \in \mathcal{T}_h \mid \text{card}(\mathcal{E}_K \cap \mathcal{E}_H) = 2\} \cup \{K \in \mathcal{T}_h \mid x^* \in \overline{K}\}. \end{aligned}$$

Notice that triangles in  $\mathcal{K}_0$  are either non-enriched (triangles of type 1 in Figure 3) or partially enriched (triangles of type 2 in Figure 3) but are in this case entirely contained in  $\Omega^+$  or  $\Omega^-$ . Triangles in  $\mathcal{K}_H$  (triangles of type 3 in Figure 3) are totally enriched. We further denote by  $K^*$  the triangle containing the crack tip  $x^*$ . Then  $\mathcal{K}^*$  contains the crack tip triangle  $K^*$  (triangle of type 5 in Figure 3) and the only triangle which is partially enriched and cut by the crack (triangle of type 4 in Figure 3). Without restriction of the generality, we exclude in this configuration the "pathological situation" where the crack tip lies on an edge or does correspond to a node of the mesh. We also exclude the case where an edge overlaps the crack or is contained in the latter. The numerical implementation of the method is able to handle these particular cases and the results of the mathematical analysis are not affected.

Let us consider the following function of Heaviside type:

$$(8) \quad H(\mathbf{x}) = \begin{cases} +1 & \text{if } (\mathbf{x} - \mathbf{x}^*) \cdot \mathbf{n}_\Sigma > 0 \\ -1 & \text{elsewhere.} \end{cases}$$

The discretization space of the XFEM-edge elements is then defined as follows:

$$(9) \quad \mathbf{X}_h^{\text{XFEM}} = \mathbf{X}_h^{\text{FE}} \oplus \text{Vect}(H\mathbf{w}_e | e \in \mathcal{E}_H) \oplus \text{Vect}(\text{grad}(\eta_\alpha S_\alpha) | \alpha \in \mathcal{I}).$$

In order to discretize the boundary value problem, we need to take into account the boundary condition on  $\Gamma$ :

$$(10) \quad \mathbf{V}_h^{\text{XFEM}} = \text{Vect}(\mathbf{w}_e | e \in \mathcal{E} \setminus \Gamma) \oplus \text{Vect}(H\mathbf{w}_e | e \in \mathcal{E}_H \setminus \Gamma) \oplus \text{Vect}(\text{grad}(\eta_\alpha S_\alpha) | \alpha \in \mathcal{I}).$$

According to the following proposition, XFEM-edge elements are conforming in  $\mathcal{H}(\text{curl}; \Omega)$ .

**Proposition 2.** *For a given triangulation  $\mathcal{T}_h$ , let  $\mathbf{X}_h^{\text{XFEM}}$  (resp.  $\mathbf{V}_h^{\text{XFEM}}$ ) be defined by (9) (resp. (10)). Then*

$$\mathbf{X}_h^{\text{XFEM}} \subset \mathcal{H}(\text{curl}; \Omega) \text{ and } \mathbf{V}_h^{\text{XFEM}} \subset \mathcal{H}_{0,\Gamma}(\text{curl}; \Omega).$$

*Proof.* We deduce from the definitions of  $\mathbf{X}_h^{\text{FE}}$  and the singular fields  $\text{grad}(\eta_\alpha S_\alpha)$  that

$$\mathbf{X}_h^{\text{FE}} \oplus \text{Vect}(\text{grad}(\eta_\alpha S_\alpha) | \alpha \in \mathcal{I}) \subset \mathcal{H}(\text{curl}; \Omega).$$

Now, let  $e \in \mathcal{E}_H$ . It follows from the enrichment strategy that  $\text{supp}(\mathbf{w}_e) \cap \Omega$  is cut by the crack into two parts. Hence, for any test function  $\varphi \in \mathcal{D}(\Omega)$ , the set  $\mathcal{O}_e$  defined by  $\mathcal{O}_e = \text{supp}(\mathbf{w}_e) \cap \text{supp}\varphi$ , splits into two closed disjoint sets  $\mathcal{O}_e^+ = \mathcal{O}_e \cap \Omega^+$  and  $\mathcal{O}_e^- = \mathcal{O}_e \cap \Omega^-$ . We have

$$\begin{aligned} \langle \text{curl } H\mathbf{w}_e, \varphi \rangle &= (H\mathbf{w}_e, \mathbf{curl} \varphi) \\ &= (\mathbf{w}_e, \mathbf{curl} \varphi)_{\mathcal{O}_e^+} - (\mathbf{w}_e, \mathbf{curl} \varphi)_{\mathcal{O}_e^-} \\ &= (H \text{curl } \mathbf{w}_e, \varphi) \end{aligned}$$

since on the boundary  $\partial\mathcal{O}^\pm$  either  $\mathbf{w}_e \times \mathbf{n}$  or  $\varphi$  vanish. This proves that  $\text{curl}(H\mathbf{w}_e)$  belongs to  $L^2(\Omega)$  with  $\text{curl}(H\mathbf{w}_e) = H \text{curl } \mathbf{w}_e$ , and thus  $\mathbf{X}_h^{\text{XFEM}} \subset \mathcal{H}(\text{curl}; \Omega)$ .

It follows from the properties of the classical edge elements that the definition of  $\mathbf{V}_h^{\text{XFEM}}$  is conforming in  $\mathcal{H}_{0,\Gamma}(\text{curl};\Omega)$ .  $\square$

The discrete problem can be written as follows

$$(\mathcal{P}_h) \quad \begin{cases} \text{Find } \mathbf{u}_h \in \mathbf{V}_h^{\text{XFEM}} \text{ such that} \\ (\mu_r^{-1} \text{curl } \mathbf{u}_h, \text{curl } \mathbf{v}_h) - \kappa^2(\varepsilon_r \mathbf{u}_h, \mathbf{v}_h) = (\mathbf{f}, \mathbf{v}_h) \quad \forall \mathbf{v}_h \in \mathbf{V}_h^{\text{XFEM}}. \end{cases}$$

We now aim to define an appropriate interpolation operator for the XFEM-edge elements. This will be done with the help of the extension operators  $\mathbf{E}^\pm$  for vector fields defined in Appendix A. These operators are continuous from  $H^s(\Omega^\pm)^2$  into  $H^s(Q)^2$  for any  $s \in [0, 2]$  and from  $H^s(\text{curl}, \Omega^\pm)$  into  $H^s(\text{curl}, \Omega)$  for any  $s \in [0, 1]$  (see Propositions 5 and 6), where  $H^s(\text{curl}, \Omega)$  denotes the subspace of  $\mathcal{H}(\text{curl};\Omega)$  of fields  $\mathbf{v}$  satisfying  $\text{curl } \mathbf{v} \in H^s(\Omega)$ .

Let  $\mathbf{u} \in \mathcal{H}_{0,\Gamma}(\text{curl};\Omega)$  such that

$$(11) \quad \mathbf{u} = \mathbf{u}_r + \sum_{\alpha \in \mathcal{I}} c_\alpha \text{grad}(\eta_\alpha S_\alpha)$$

with  $\mathbf{u}_r \in H^1(\Omega)^2$ . The XFEM-interpolant of the regular part is defined as follows:

$$(12) \quad \mathbf{r}_h^{\text{XFEM}} \mathbf{u}_r = \sum_{e \in \mathcal{E}} a_e \mathbf{w}_e + \sum_{e \in \mathcal{E}_H} b_e H \mathbf{w}_e$$

where  $a_e = l_e(\mathbf{u}_r)$  if  $e \in \mathcal{E} \setminus \mathcal{E}_H$  and

$$(13) \quad \begin{aligned} a_e &= \frac{1}{2} \left( \int_e \gamma_e(\mathbf{E}^+ \mathbf{u}_r) \cdot \mathbf{t}_e \, ds + \int_e \gamma_e(\mathbf{E}^- \mathbf{u}_r) \cdot \mathbf{t}_e \, ds \right) \\ b_e &= \frac{1}{2} \left( \int_e \gamma_e(\mathbf{E}^+ \mathbf{u}_r) \cdot \mathbf{t}_e \, ds - \int_e \gamma_e(\mathbf{E}^- \mathbf{u}_r) \cdot \mathbf{t}_e \, ds \right) \end{aligned}$$

if  $e \in \mathcal{E}_H$ . The XFEM-interpolant of  $\mathbf{u}$  is then given by

$$(14) \quad \mathbf{r}_h^{\text{XFEM}} \mathbf{u} = \mathbf{r}_h^{\text{XFEM}} \mathbf{u}_r + \sum_{\alpha \in \mathcal{I}} c_\alpha \text{grad}(\eta_\alpha S_\alpha).$$

The local XFEM-interpolant on a triangle  $K \in \mathcal{T}_h$  is defined by restriction of  $\mathbf{r}_h^{\text{XFEM}} \mathbf{u}$  to  $K$ .

#### 4. Error estimates for the interpolation error

In this section we prove error estimates for the interpolation error  $\mathbf{u} - \mathbf{r}_h^{\text{XFEM}} \mathbf{u}$  in the energy norm  $\|\cdot\|_{\mathcal{H}(\text{curl};\Omega)}$ . Here,  $\mathbf{u}$  is a vector field in  $\mathcal{H}(\text{curl};\Omega)$  that splits into a regular part  $\mathbf{u}_r$  and a singular part according to (11). We recall that

$$(15) \quad \mathcal{H}^s(\text{curl};\Omega) = \{ \mathbf{u} \in H^s(\Omega)^2 \mid \text{curl } \mathbf{u} \in H^s(\Omega) \}.$$

We consider a regular family of triangulations  $(\mathcal{T}_h)_{h>0}$  in the sense of [10]: for any triangle  $K \in \cup_h \mathcal{T}_h$ , we define the parameters  $h_K$  and  $\rho_K$  such that  $h_K$  is the diameter of  $K$  and  $\rho_K$  denotes the diameter of the largest sphere contained in  $K$ . The mesh parameter  $h$  is given by  $h = \max_{K \in \mathcal{T}_h} h_K$  and tends to zero. Then, we assume that there is a constant  $\sigma_{\min} > 0$  such that

$$\forall K \in \cup_h \mathcal{T}_h, \quad \frac{h_K}{\rho_K} \geq \sigma_{\min}.$$

The interpolation error estimate reads as follows.

**Theorem 4.** *Assume that  $\mathbf{u} \in \mathcal{H}(\text{curl}; \Omega)$  admits the decomposition (11). Assume further that the regular part  $\mathbf{u}_r$  belongs to  $\mathcal{H}^s(\text{curl}; \Omega)$  with  $\frac{1}{2} < s \leq 1$  and that  $\mathbf{u}_r \in H^{1+\sigma}(\Omega)^2$  with  $\sigma > 0$ . Then, there is a disk  $B(x^*, ch) \subset \Omega$  of radius  $ch$  (with  $c > 0$  a constant independent from the mesh) centered at the crack tip  $x^*$  such that the following estimate holds true,*

$$(16) \quad \left\| \mathbf{u} - \mathbf{r}_h^{\text{XFEM}} \mathbf{u} \right\|_{\mathcal{H}(\text{curl}; \Omega)} \lesssim h^s \|\mathbf{u}_r\|_{\mathcal{H}^s(\text{curl}; \Omega)} + h^\sigma |\mathbf{u}_r|_{1+\sigma, B(x^*, ch) \cap \Omega}.$$

Here and throughout the rest of the paper, the notation  $a \lesssim b$  means that there is a constant  $C > 0$  independent of the meshsize  $h$  and of the function under consideration such that  $a \leq Cb$ .

*Proof.* We have

$$(17) \quad \mathbf{u} - \mathbf{r}_h^{\text{XFEM}} \mathbf{u} = \mathbf{u}_r - \mathbf{r}_h^{\text{XFEM}} \mathbf{u}_r$$

since the singular part of  $\mathbf{u}$  is taken into account exactly according to (14). We thus need to prove error estimates only for the regular part  $\mathbf{u}_r$ . Lemmas 1, 2 and 3 hereafter give interpolation error estimates locally on the different type of triangles defined in §3 (see Figure 3). Putting these results together, we get

$$\begin{aligned} & \left\| \mathbf{u}_r - \mathbf{r}_h^{\text{XFEM}} \mathbf{u}_r \right\|_{\mathcal{H}(\text{curl}; \Omega)}^2 \\ & \lesssim h^{2s} \sum_{K \in \mathcal{K}_0} \|\mathbf{u}_r\|_{\mathcal{H}^s(\text{curl}; K)}^2 \\ & \quad + h^{2s} \sum_{K \in \mathcal{K}_H \cup \mathcal{K}^*} \left( \|\mathbf{E}^+ \mathbf{u}_r\|_{\mathcal{H}^s(\text{curl}; K)}^2 + \|\mathbf{E}^- \mathbf{u}_r\|_{\mathcal{H}^s(\text{curl}; K)}^2 \right) \\ & \quad + h^{2\sigma} \sum_{K \in \mathcal{K}^*} |\mathbf{u}_r|_{1+\sigma, B(x^*, ch) \cap \Omega}^2. \end{aligned}$$

Now, the restriction of the extended fields  $\mathbf{E}^\pm \mathbf{u}_r$  on  $K$  depends continuously on the values of  $\mathbf{u}_r$  on a rectangle of measure  $\mathcal{O}(h^2)$  containing  $K$ . Hence,

$$\sum_{K \in \mathcal{K}_H \cup \mathcal{K}^*} \left( \|\mathbf{E}^+ \mathbf{u}_r\|_{\mathcal{H}^s(\text{curl}; K)}^2 + \|\mathbf{E}^- \mathbf{u}_r\|_{\mathcal{H}^s(\text{curl}; K)}^2 \right) \lesssim \|\mathbf{u}_r\|_{\mathcal{H}^s(\text{curl}; \Omega)}^2.$$

We further notice that the set  $\mathcal{K}^*$  contains exactly two triangles and thus

$$\sum_{K \in \mathcal{K}^*} |\mathbf{u}_r|_{1+\sigma, B(x^*, ch) \cap \Omega}^2 \lesssim |\mathbf{u}_r|_{1+\sigma, B(x^*, ch) \cap \Omega}^2$$

independently from the mesh. This proves estimate (16).  $\square$

We now prove interpolation error estimates locally on the different type of triangles. The first lemma deals with non-enriched triangles or partially enriched triangles that are completely contained in  $\Omega^+$  or  $\Omega^-$ .

**Lemma 1.** *Assume that  $\mathbf{u} \in \mathcal{H}(\text{curl}; \Omega)$  admits the decomposition (11). Assume further that the regular part  $\mathbf{u}_r$  belongs to  $\mathcal{H}^s(\text{curl}; \Omega)$  with  $\frac{1}{2} < s \leq 1$ . Let  $K \in \mathcal{K}_0$ . Then*

$$(18) \quad \left\| \mathbf{u}_r - \mathbf{r}_K^{\text{XFEM}} \mathbf{u}_r \right\|_{\mathcal{H}(\text{curl}; K)} \leq Ch^s \|\mathbf{u}_r\|_{\mathcal{H}^s(\text{curl}; K)}.$$

*Proof.* If  $K$  is non-enriched, the restriction of  $\mathbf{r}_h^{\text{XFEM}} \mathbf{u}_r$  to  $K$  does coincide with the interpolant of classical edge elements. Hence, we deduce from classical error estimates (see e.g. [25]) that

$$\left\| \mathbf{u}_r - \mathbf{r}_K^{\text{XFEM}} \mathbf{u}_r \right\|_{\mathcal{H}(\text{curl}; K)} = \left\| \mathbf{u}_r - \mathbf{r}_K^{\text{FE}} \mathbf{u}_r \right\|_{\mathcal{H}(\text{curl}; K)} \lesssim h^s \|\mathbf{u}_r\|_{\mathcal{H}^s(\text{curl}; K)}.$$

If  $K$  is partially enriched but does not intersect the crack, say  $K \subset \Omega^+$ , we have

$$\begin{aligned} r_K^{\text{XFEM}} \mathbf{u}_r &= \sum_{e \in \partial K: e \in \mathcal{E}_H} (a_e + b_e) \mathbf{w}_e^K + \sum_{e \in \partial K: e \in \mathcal{E} \setminus \mathcal{E}_H} a_e \mathbf{w}_e^K \\ &= \sum_{e \in \partial K: e \in \mathcal{E}_H} l_e(\mathbf{E}^+ \mathbf{u}_r) \mathbf{w}_e^K + \sum_{e \in \partial K: e \in \mathcal{E} \setminus \mathcal{E}_H} l_e(\mathbf{u}_r) \mathbf{w}_e^K \\ &= r_K^{\text{FE}} \mathbf{u}_r \end{aligned}$$

since  $\mathbf{E}^+ \mathbf{u}_r = \mathbf{u}_r$  on  $\Omega^+$ . Estimate (18) follows again from classical error estimates.  $\square$

On totally enriched elements  $K$ , the XFEM-interpolant involves the extension operators  $\mathbf{E}^\pm$ . We have the following

**Lemma 2.** *Assume that  $\mathbf{u} \in \mathcal{H}(\text{curl}; \Omega)$  admits the decomposition (11). Assume further that the regular part  $\mathbf{u}_r$  belongs to  $\mathcal{H}^s(\text{curl}; \Omega)$  with  $\frac{1}{2} < s \leq 1$ . Let  $K \in \mathcal{K}_H$ . Then*

$$(19) \quad \|\mathbf{u}_r - r_K^{\text{XFEM}} \mathbf{u}_r\|_{\mathcal{H}(\text{curl}; K \cap \Omega)} \lesssim h^s \left( \|\mathbf{E}^+ \mathbf{u}_r\|_{\mathcal{H}^s(\text{curl}; K)}^2 + \|\mathbf{E}^- \mathbf{u}_r\|_{\mathcal{H}^s(\text{curl}; K)}^2 \right)^{1/2}.$$

*Proof.* According to the properties of the extension operators  $\mathbf{E}^\pm$  (see Proposition 6), we have

$$\mathbf{E}^\pm \in \mathcal{H}^s(\text{curl}; Q).$$

We compute  $r_K^{\text{XFEM}} \mathbf{u}_r$  separately on  $K^+ = K \cap \overline{\Omega^+}$  and  $K^- = K \cap \overline{\Omega^-}$ :

$$(r_K^{\text{XFEM}} \mathbf{u}_r)|_{K^+} = \sum_{e \in \partial K} (a_e + b_e) \mathbf{w}_{e|K^+}^K = \sum_{e \in \partial K} l_e(\mathbf{E}^+ \mathbf{u}_r) \mathbf{w}_{e|K^+}^K = (r_K^{\text{FE}} \mathbf{E}^+ \mathbf{u}_r)|_{K^+}$$

and in the same way

$$(r_K^{\text{XFEM}} \mathbf{u}_r)|_{K^-} = (r_K^{\text{FE}} \mathbf{E}^- \mathbf{u}_r)|_{K^-}.$$

Taking into account that  $\mathbf{u}_r|_{K^\pm} = (\mathbf{E}^\pm \mathbf{u}_r)|_{K^\pm}$ , it follows from classical error estimates for the extended fields  $\mathbf{E}^\pm \mathbf{u}_r$  that

$$\begin{aligned} &\|\mathbf{u}_r - r_K^{\text{XFEM}} \mathbf{u}_r\|_{\mathcal{H}(\text{curl}; K \cap \Omega)}^2 \\ &= \|\mathbf{E}^+ \mathbf{u}_r - r_K^{\text{FE}} \mathbf{E}^+ \mathbf{u}_r\|_{\mathcal{H}(\text{curl}; K^+)}^2 + \|\mathbf{E}^- \mathbf{u}_r - r_K^{\text{FE}} \mathbf{E}^- \mathbf{u}_r\|_{\mathcal{H}(\text{curl}; K^-)}^2 \\ &\lesssim h^{2s} \|\mathbf{E}^+ \mathbf{u}_r\|_{\mathcal{H}^s(\text{curl}; K)}^2 + h^{2s} \|\mathbf{E}^- \mathbf{u}_r\|_{\mathcal{H}^s(\text{curl}; K)}^2. \end{aligned}$$

$\square$

The situation is more involved if  $K$  is partially enriched or does coincide with the crack tip triangle.

**Lemma 3.** *Assume that  $\mathbf{u} \in \mathcal{H}(\text{curl}; \Omega)$  admits the decomposition (11). Assume further that the regular part  $\mathbf{u}_r$  belongs to  $H^{1+\sigma}(\Omega)^2$  with  $\sigma > 0$  and that  $\text{curl} \mathbf{u}_r$  belongs to  $H^s(\Omega)$  with  $\frac{1}{2} < s \leq 1$ . Let  $K \in \mathcal{K}^*$ . Then there is a rectangle  $Q_K$  satisfying  $K \subset Q_K$  and  $\text{meas}(Q_K) = \mathcal{O}(h^2)$  and a constant  $c > 0$  such that*

$$(20) \quad \|\mathbf{u}_r - r_K^{\text{XFEM}} \mathbf{u}_r\|_{\mathcal{H}(\text{curl}; K \cap \Omega)} \lesssim h^s \|\mathbf{u}_r\|_{\mathcal{H}^s(\text{curl}; Q_K \cap \Omega)} + h^\sigma |\mathbf{u}_r|_{1+\sigma, B(x^*, ch) \cap \Omega},$$

where  $B(x^*, ch)$  denotes a disk centered at the crack tip  $x^*$  with radius  $ch$ .

*Proof.* We compute  $r_K^{\text{XFEM}} \mathbf{u}_r$  separately on  $K^+$  and  $K^-$ . According to the definition of  $r_K^{\text{XFEM}}$ , we have

$$\begin{aligned} (r_K^{\text{XFEM}} \mathbf{u}_r)|_{K^+} &= \sum_{e \in \partial K: e \in \mathcal{E}_H} l_e(\mathbf{E}^+ \mathbf{u}_r) \mathbf{w}_e^K|_{K^+} + \sum_{e \in \partial K: e \notin \mathcal{E}_H} l_e(\mathbf{u}_r) \mathbf{w}_e^K|_{K^+} \\ &= \sum_{e \in \partial K} l_e(\mathbf{E}^+ \mathbf{u}_r) \mathbf{w}_e^K|_{K^+} + \sum_{e \in \partial K: e \notin \mathcal{E}_H} l_e(\mathbf{u}_r - \mathbf{E}^+ \mathbf{u}_r) \mathbf{w}_e^K|_{K^+} \\ &= (r_K^{\text{FE}} \mathbf{E}^+ \mathbf{u}_r)|_{K^+} + \sum_{e \in \partial K: e \notin \mathcal{E}_H} l_e(\mathbf{u}_r - \mathbf{E}^+ \mathbf{u}_r) \mathbf{w}_e^K|_{K^+}. \end{aligned}$$

On  $K^-$ , we get in the same way

$$(r_K^{\text{XFEM}} \mathbf{u}_r)|_{K^-} = (r_K^{\text{FE}} \mathbf{E}^- \mathbf{u}_r)|_{K^-} + \sum_{e \in \partial K: e \notin \mathcal{E}_H} l_e(\mathbf{u}_r - \mathbf{E}^- \mathbf{u}_r) \mathbf{w}_e^K|_{K^-}.$$

Thus,

$$\begin{aligned} (21) \quad & \|\mathbf{u} - r_K^{\text{XFEM}} \mathbf{u}\|_{\mathcal{H}(\text{curl}; K \cap \Omega)} \\ & \lesssim \|\mathbf{E}^+ \mathbf{u}_r - r_K^{\text{FE}} \mathbf{E}^+ \mathbf{u}_r\|_{\mathcal{H}(\text{curl}; K^+)} + \|\mathbf{E}^- \mathbf{u}_r - r_K^{\text{FE}} \mathbf{E}^- \mathbf{u}_r\|_{\mathcal{H}(\text{curl}; K^-)} \\ & \quad + \sum_{e \in \partial K: e \notin \mathcal{E}_H} (|l_e(\mathbf{u}_r - \mathbf{E}^+ \mathbf{u}_r)| + |l_e(\mathbf{u}_r - \mathbf{E}^- \mathbf{u}_r)|) \|\mathbf{w}_e^K\|_{\mathcal{H}(\text{curl}; K)} \\ & \lesssim h^s \left( \|\mathbf{E}^+ \mathbf{u}_r\|_{\mathcal{H}^s(\text{curl}; K)} + \|\mathbf{E}^- \mathbf{u}_r\|_{\mathcal{H}^s(\text{curl}; K)} \right) \\ (22) \quad & + \sum_{e \in \partial K: e \notin \mathcal{E}_H} (|l_e(\mathbf{u}_r - \mathbf{E}^+ \mathbf{u}_r)| + |l_e(\mathbf{u}_r - \mathbf{E}^- \mathbf{u}_r)|) \|\mathbf{w}_e^K\|_{\mathcal{H}(\text{curl}; K)} \end{aligned}$$

where we used classical error estimates for the interpolation error  $\mathbf{E}^\pm \mathbf{u}_r - r_K^{\text{FE}} \mathbf{E}^\pm \mathbf{u}_r$ .

We recall the definition of the local basis function associated with the edge  $e$ ,

$$\mathbf{w}_e^K = (B_K^t)^{-1} \hat{\mathbf{w}}_e$$

where the affine application  $F_K : \hat{K} \rightarrow K$  that maps the reference triangle  $\hat{K}$  onto  $K$ , is given by  $F_K(\hat{\mathbf{x}}) = B_K \mathbf{x} + \mathbf{b}_K$  with a non-singular matrix  $B_K \in \mathcal{M}_2(\mathbb{R})$  and a vector  $\mathbf{b}_K \in \mathbb{R}^2$ . Notice that in two dimensions of space the curl transforms in the following way,

$$\text{curl } \mathbf{w}_e^K \circ F_K = \frac{1}{\det B_K} \hat{\text{curl}} \hat{\mathbf{w}}_e.$$

We thus have  $\|\mathbf{w}_e^K\|_{0,K} = \mathcal{O}(1)$  and  $\|\text{curl } \mathbf{w}_e^K\|_{0,K} = \mathcal{O}(h_K^{-1})$ .

Now, let  $e$  be a non enriched edge of a triangle of type 5 or 6. Such an edge necessarily belongs to the crack tip triangle and we thus can apply Lemma 4. Hence, there is a constant  $c > 0$  such that

$$|l_e(\mathbf{u}_r - \mathbf{E}^\pm \mathbf{u}_r)| \lesssim h_K^{1+\sigma} |\mathbf{u}_r|_{1+\sigma, B(\mathbf{x}^*, ch) \cap \Omega}.$$

Using this estimate in (22) yields (20) since  $\|\mathbf{w}_e^K\|_{\mathcal{H}(\text{curl}; K)} = \mathcal{O}(h_K^{-1})$  and  $\mathbf{E}^\pm \mathbf{u}_r|_K$  depends continuously on the values of  $\mathbf{u}_r$  in a rectangle  $Q_K$  containing  $K$  and such that  $\text{meas}(Q) = \mathcal{O}(h^2)$ .  $\square$

**Lemma 4.** *Assume that  $e \in \mathcal{E}$  is an edge belonging to the crack tip triangle  $K^*$ . Under the assumptions of Lemma 3 there is a constant  $c > 0$  such that the following estimate holds true,*

$$|l_e(\mathbf{u}_r - \mathbf{E}^\pm \mathbf{u}_r)| \lesssim h_{K^*}^{1+\sigma} |\mathbf{u}_r|_{1+\sigma, B(\mathbf{x}^*, ch) \cap \Omega}.$$

*Proof.* Let  $\mathbf{v} = \mathbf{u}_r - \mathbf{E}^+ \mathbf{u}_r$ .  $\mathbf{v}$  belongs to  $H^{1+\sigma}(K^* \cap \Omega)^2$  and  $\mathbf{v} \equiv 0$  on  $K^* \cap \Omega^+$ . In general,  $\mathbf{v}$  will be discontinuous across  $\Sigma \cap K^*$ , but is continuous over  $\mathcal{D} \setminus \Sigma$ . By the embedding  $H^{1+\sigma}(K^* \cap \Omega)^2 \hookrightarrow \mathcal{C}^0(\overline{K^*} \cap \Omega)^2$  and the regularity of the mesh, we may write

$$|l_e(\mathbf{v})| \lesssim h_e \|\mathbf{v}\|_{\infty, B(\mathbf{x}^*, h) \cap \Omega}.$$

By a scaling argument, and since  $\mathbf{v} \equiv 0$  on  $K^* \cap \Omega^+$ , we have

$$\|\mathbf{v}\|_{\infty, B(\mathbf{x}^*, h) \cap \Omega} = \|\hat{\mathbf{v}}\|_{\infty, B(0,1) \setminus F_{K^*}^{-1}(\Sigma)} \lesssim |\hat{\mathbf{v}}|_{1+\sigma, B(0,1) \setminus F_{K^*}^{-1}(\Sigma)},$$

where  $\hat{\mathbf{v}}(\hat{r}, \hat{\theta}) = \mathbf{v}(r, \theta)$  with  $(r, \theta) = (h\hat{r}, \hat{\theta})$ . Another scaling argument together with the continuity of the extension operator then yields the assertion.  $\square$

Now, C ea’s lemma and Theorem 4 yield the following estimate of the discretization error.

**Corollary 2.** *Let  $\mathbf{u} \in \mathcal{H}_{0,\Gamma}(\text{curl}; \Omega)$  be the solution of problem (P) and let  $\mathbf{u}_h \in \mathbf{V}_h^{\text{XFEM}}$  be the discrete solution of problem (P<sub>h</sub>). Then*

$$(23) \quad \|\mathbf{u} - \mathbf{u}_h\|_{\mathcal{H}(\text{curl}; \Omega)} \lesssim h^{1/2-\eta} (\|\mathbf{u}_r\|_{\mathcal{H}^1(\text{curl}; \Omega)} + |\mathbf{u}_r|_{3/2-\eta, B(\mathbf{x}^*, ch) \cap \Omega})$$

where  $\mathbf{u}_r \in H^{3/2-\eta}(\Omega)^2$  denotes the regular part of the exact solution  $\mathbf{u}$ .

Theorem 4 does not apply in the limit case when the regular part only has the  $H^1$ -regularity. However, we still can prove the following convergence result for the interpolation error in the  $L^2$ -norm.

**Proposition 3.** *Assume that  $\mathbf{u} \in \mathcal{H}(\text{curl}; \Omega)$  admits a decomposition according to (11) with  $\mathbf{u}_r \in H^1(\Omega)^2$ . Then,*

$$\lim_{h \rightarrow 0} \|\mathbf{u} - r_h^{\text{XFEM}} \mathbf{u}\|_{0, \Omega} = 0.$$

*Proof.* As before, we have

$$\|\mathbf{u} - r_h^{\text{XFEM}} \mathbf{u}\|_{0, \Omega} = \|\mathbf{u}_r - r_h^{\text{XFEM}} \mathbf{u}_r\|_{0, \Omega},$$

and we only have to estimate the interpolation error for the regular part  $\mathbf{u}_r$ . Now, let  $\varepsilon > 0$ . Using standard density results, there is a field  $\mathbf{u}_r^\varepsilon \in H^2(\Omega)^2$  such that  $\|\mathbf{u}_r - \mathbf{u}_r^\varepsilon\|_{1, \Omega} < \varepsilon$ . According to Theorem 4, we have

$$\|\mathbf{u}_r^\varepsilon - r_h^{\text{XFEM}} \mathbf{u}_r^\varepsilon\|_{\mathcal{H}(\text{curl}; \Omega)} \leq Ch \|\mathbf{u}_r^\varepsilon\|_{2, \Omega}.$$

Let  $h_0 > 0$  be such that

$$Ch_0 \|\mathbf{u}_r^\varepsilon\|_{2, \Omega} < \varepsilon.$$

Then,

$$\begin{aligned} & \|\mathbf{u}_r - r_h^{\text{XFEM}} \mathbf{u}_r\|_{0, \Omega} \\ & \leq \|\mathbf{u}_r - \mathbf{u}_r^\varepsilon\|_{0, \Omega} + \|\mathbf{u}_r^\varepsilon - r_h^{\text{XFEM}} \mathbf{u}_r^\varepsilon\|_{0, \Omega} + \|r_h^{\text{XFEM}} \mathbf{u}_r^\varepsilon - r_h^{\text{XFEM}} \mathbf{u}_r\|_{0, \Omega} \\ & \leq 2\varepsilon + \|r_h^{\text{XFEM}} \mathbf{u}_r^\varepsilon - r_h^{\text{XFEM}} \mathbf{u}_r\|_{0, \Omega}. \end{aligned}$$

The result follows from the continuity of the interpolation operator  $r_h^{\text{XFEM}}$  as a linear application from  $H^1(\Omega)^2$  into  $L^2(\Omega)^2$  which is proved in Lemma 5 hereafter.  $\square$

**Lemma 5.** *Let  $\mathbf{v} \in H^1(\Omega)^2$ . Then there exists a constant  $C > 0$  independent from  $\mathbf{v}$  and  $h$  such that*

$$\|r_h^{\text{XFEM}} \mathbf{v}\|_{0, \Omega} \leq C \|\mathbf{v}\|_{1, \Omega}^2.$$

*Proof.* Let  $\mathbf{v} \in H^1(\Omega)^2$ . We deduce from the definition of  $r_h^{\text{XFEM}}$  that

$$\begin{aligned} \|r_h^{\text{XFEM}} \mathbf{v}\|_{0,\Omega}^2 &\lesssim \sum_{K \in \mathcal{K}_0} \|r_K^{\text{FE}} \mathbf{v}\|_{0,K}^2 + \sum_{K \in \mathcal{K}_H \cup \mathcal{K}^*} \left( \|r_K^{\text{FE}} \mathbf{E}^+ \mathbf{v}\|_{0,K}^2 + \|r_K^{\text{FE}} \mathbf{E}^- \mathbf{v}\|_{0,K}^2 \right) \\ &\quad + \sum_{K \in \mathcal{K}^*} \sum_{e \in \partial K: e \notin \mathcal{E}_H} (|l_e(\mathbf{v} - \mathbf{E}^+ \mathbf{v})|^2 + |l_e(\mathbf{v} - \mathbf{E}^- \mathbf{v})|^2) \|\mathbf{w}_e\|_{0,K}^2 \end{aligned}$$

Now, let  $K \in \mathcal{K}_0$ . According to the definition of  $r_K^{\text{FE}}$ , we have

$$r_K^{\text{FE}} \mathbf{v} = \sum_{e=1}^3 l_e(\mathbf{v}) \mathbf{w}_e.$$

Hence,

$$\|r_K^{\text{FE}} \mathbf{v}\|_{0,K}^2 = \int_K \left| \sum_{e=1}^3 l_e(\mathbf{v}) \mathbf{w}_e \right|^2 dx \lesssim \sum_{e=1}^3 |l_e(\mathbf{v})|^2$$

since  $\|\mathbf{w}_e\|_{0,K} = \mathcal{O}(1)$ . But  $l_e(\mathbf{v}) = \hat{l}_e(\hat{\mathbf{v}})$  where  $\hat{\mathbf{v}}(\hat{\mathbf{x}}) = B_K^t \mathbf{v}(\mathbf{x})$  is defined on the reference triangle  $\hat{K}$  according to the transformation  $\mathbf{x} = B_K \hat{\mathbf{x}} + \mathbf{b}_K$ . This implies that

$$\|r_K^{\text{FE}} \mathbf{v}\|_{0,K}^2 \lesssim \sum_{\hat{e}=1}^3 \left| \hat{l}_{\hat{e}}(\hat{\mathbf{v}}) \right|^2 \lesssim \sum_{\hat{e}=1}^3 \|\hat{\mathbf{v}}\|_{0,\hat{e}}^2 = \|\hat{\mathbf{v}}\|_{0,\partial \hat{K}}^2.$$

Then the trace theorem yields

$$\|\hat{\mathbf{v}}\|_{0,\partial \hat{K}} \lesssim \|\hat{\mathbf{v}}\|_{1,\hat{K}}$$

where we notice that the involved constant only depends on the reference triangle and is thus independent from  $h$ . Going back to the triangle  $K$  in the physical domain yields

$$|\hat{\mathbf{v}}|_{s,\hat{K}} \lesssim h_K^s |\mathbf{v}|_{s,K} \quad \forall s \text{ such that } 0 \leq s \leq 1$$

and finally

$$(24) \quad \|r_K^{\text{FE}} \mathbf{v}\|_{0,K} \lesssim \|\mathbf{v}\|_{1,K}.$$

In the same way, we get for a triangle  $K \in \mathcal{K}_H \cup \mathcal{K}^*$ ,

$$(25) \quad \|r_K^{\text{FE}} \mathbf{E}^\pm \mathbf{v}\|_{0,K^\pm} \lesssim \|\mathbf{E}^\pm \mathbf{v}\|_{1,K}.$$

Finally, let  $K \in \mathcal{K}^*$ . We have

$$\begin{aligned} \sum_{e \in \partial K: e \notin \mathcal{E}_H} |l_e(\mathbf{v} - \mathbf{E}^\pm \mathbf{v})|^2 \|\mathbf{w}_e\|_{0,K}^2 &\lesssim \sum_{e \in \partial K: e \notin \mathcal{E}_H} |l_e(\mathbf{v})|^2 + |l_e(\mathbf{E}^\pm \mathbf{v})|^2 \\ &\lesssim \|\mathbf{v}\|_{1,K}^2 + \|\mathbf{E}^\pm \mathbf{v}\|_{1,K}^2 \end{aligned}$$

using the same argument as before. Summing up over  $K$  then yields the result taking into account the continuity of the extension operators  $\mathbf{E}^\pm$ .  $\square$

## 5. Numerical results

In this section, we will discuss the numerical implementation of our eXtended Finite Element Method for edge elements. In order to simplify the presentation, the non-cracked domain  $\bar{Q}$  will be chosen to be the square  $[-0.5, 0.5] \times [-0.5, 0.5]$  and we suppose that the crack is supported by the  $x_1$ -axis,

$$\Sigma = [-\delta, 0.5] \times \{0\}$$

where  $0 < \delta < 0.5$  is a small parameter. We consider a regular family  $(\mathcal{T}_h)_{h>0}$  of structured triangulations of  $\bar{Q}$ . The parameter  $\delta$  is chosen in such a way that the crack tip  $\mathbf{x}^* = (-\delta, 0)$  does never lie on any edge of the triangulations. This choice

allows to test the method in the most current configuration where the crack tip is situated in the interior of a single triangle. The implementation of the method, however, can handle any location of the crack segment. According to the configuration of the crack, only the singular function  $S_1$  localized at the crack tip has to be taken into account.

We recall that the discrete problem  $(\mathcal{P}_h)$  in §3 is given by

$$(\mathcal{P}_h) \quad \begin{cases} \text{Find } \mathbf{u}_h \in \mathbf{V}_h^{\text{XFEM}} \text{ such that} \\ a(\mathbf{u}_h, \mathbf{v}_h) = l(\mathbf{v}_h) \quad \forall \mathbf{v}_h \in \mathbf{V}_h^{\text{XFEM}} \end{cases}$$

on the space

$$\mathbf{V}_h^{\text{XFEM}} = \text{Vect}(\mathbf{w}_e | e \in \mathcal{E} \setminus \Gamma) \oplus \text{Vect}(H\mathbf{w}_e | e \in \mathcal{E}_H \setminus \Gamma) \oplus \text{Vect}(\text{grad}(\eta_1 S_1))$$

with the sesquilinear form  $a(\mathbf{u}_h, \mathbf{v}_h) = (\mu_r^{-1} \text{curl } \mathbf{u}_h, \text{curl } \mathbf{v}_h) - \kappa^2(\varepsilon_r \mathbf{u}_h, \mathbf{v}_h)$  and the linear form  $l(\mathbf{v}_h) = (\mathbf{f}, \mathbf{v}_h)$ .

Now, let  $N_h = \text{card}(\mathcal{E} \setminus \Gamma)$  be the total number of interior edges and denote by  $N_h^H = \text{card}(\mathcal{E}_H \setminus \Gamma)$  the number of enriched interior edges. It is clear that  $\mathbf{V}_h^{\text{XFEM}}$  is a finite-dimensional vector space of dimension  $N_h + N_h^H + 1$ . Hence,  $(\mathcal{P}_h)$  can be written in an equivalent manner in block matrix form,

$$(26) \quad \begin{pmatrix} \mathbb{A} & C \\ C^T & a_s \end{pmatrix} \begin{pmatrix} U_r \\ u_s \end{pmatrix} = \begin{pmatrix} F \\ f_s \end{pmatrix}$$

where

- $\mathbb{A}$  and  $F$  respectively, denote the matrix and the right-hand side corresponding to finite element terms. More precisely, the matrix  $\mathbb{A}$  and the vector  $F$  have again a block structure corresponding to the set of enriched degrees of freedom:

$$\mathbb{A} = \begin{pmatrix} \mathbb{A}^{\mathcal{E}\mathcal{E}} & \mathbb{A}^{\mathcal{E}\mathcal{E}_H} \\ \mathbb{A}^{\mathcal{E}_H\mathcal{E}} & \mathbb{A}^{\mathcal{E}_H\mathcal{E}_H} \end{pmatrix} \quad F = \begin{pmatrix} F^{\mathcal{E}} \\ F^{\mathcal{E}_H} \end{pmatrix}$$

where

$$\begin{aligned} \mathbb{A}_{ee'}^{\mathcal{E}\mathcal{E}} &= a(\mathbf{w}_{e'}, \mathbf{w}_e) & \forall e, e' \in \mathcal{E} \setminus \Gamma, \\ \mathbb{A}_{ee'}^{\mathcal{E}_H\mathcal{E}_H} &= a(H\mathbf{w}_{e'}, H\mathbf{w}_e) & \forall e, e' \in \mathcal{E}_H \setminus \Gamma, \\ \mathbb{A}_{ee'}^{\mathcal{E}\mathcal{E}_H} &= a(H\mathbf{w}_{e'}, \mathbf{w}_e) & \forall e \in \mathcal{E} \setminus \Gamma, \forall e' \in \mathcal{E}_H \setminus \Gamma, \\ \mathbb{A}_{ee'}^{\mathcal{E}_H\mathcal{E}} &= a(\mathbf{w}_{e'}, H\mathbf{w}_e) & \forall e \in \mathcal{E}_H \setminus \Gamma, \forall e' \in \mathcal{E} \setminus \Gamma \end{aligned}$$

and

$$\begin{aligned} F_e^{\mathcal{E}} &= l(\mathbf{w}_e) & \forall e \in \mathcal{E} \setminus \Gamma, \\ F_e^{\mathcal{E}_H} &= l(H\mathbf{w}_e) & \forall e \in \mathcal{E}_H \setminus \Gamma, \end{aligned}$$

- $a_s = a(\text{grad}(\eta_1 S_1), \text{grad}(\eta_1 S_1))$  and  $f_s = l(\text{grad}(\eta_1 S_1))$  denote the matrix and the right-hand side of size 1 corresponding to the singular field,
- $C$  is a matrix of size  $(N_h + N_h^H) \times 1$  coupling the basis functions of FE-type with the singular field. As does the right-hand side  $F$ ,  $C$  splits into two blocks, where the second block corresponds to the enriched degrees of freedom:

$$C = \begin{pmatrix} C^{\mathcal{E}} \\ C^{\mathcal{E}_H} \end{pmatrix}$$

with  $C_e^{\mathcal{E}} = a(\text{grad}(\eta_1 S_1), \mathbf{w}_e)$  for any  $e \in \mathcal{E} \setminus \Gamma$ , and  $C_e^{\mathcal{E}_H} = a(\text{grad}(\eta_1 S_1), H\mathbf{w}_e)$  whenever  $e$  belongs to  $\mathcal{E}_H \setminus \Gamma$ .

- $U_r$  is the vector of unknowns corresponding to basis functions of finite element type, whereas  $u_s$  is the coefficient of the singular part of the discrete solution:

$$\mathbf{u}_h(\mathbf{x}) = \sum_{e \in \mathcal{E} \setminus \Gamma} U_{r,e} \mathbf{w}_e(\mathbf{x}) + \sum_{e \in \mathcal{E}_H \setminus \Gamma} U_{r,e} H \mathbf{w}_e(\mathbf{x}) + u_s \text{grad}(\eta_1 S_1)(\mathbf{x}).$$

The block structure of the linear system (26) allows to rewrite the discrete problem in order to solve two linear systems involving the same sparse matrix  $\mathbb{A}$  corresponding to the finite element approximation. This is advantageous with regards to the storage and the conditioning of the matrix (see Table 1). The algorithm thus reads as follows (see [19] for a similar algorithm in the context of the *Singular Field Method*):

- (1) Solve the following two linear systems

$$\begin{cases} \mathbb{A}U = F \\ \mathbb{A}S = C \end{cases},$$

- (2) Compute the approximate singular coefficient by

$$u_s = \frac{f_s - C^T U}{a_s - C^T S},$$

- (3) Determine the "regular" part by

$$U_r = U - u_s S.$$

**Remark 5.** Notice that in the case where  $k$  singular functions have to be taken into account, the resolution of  $k + 1$  linear systems involving the same sparse matrix  $\mathbb{A}$  is required, and the singular coefficients are the solution of a  $k$  by  $k$  linear system which is diagonal if the supports of the cut-off functions involved in the definition of the singular fields do not intersect.

Actually, the matrix  $\mathbb{A}$  as well as the right hand sides,  $F$  and  $C$ , should be assembled for all degrees of freedom (even those supported by  $\Gamma$ ) in order to handle non-homogeneous boundary conditions which are taken into account *via* the technique of pseudo-elimination.

mesh	$h$	<i>d.o.f.</i>	$\text{cond}_2(\mathbb{A})$
#1	2.020e-01	175	4.003e+03
#2	8.319e-02	935	3.486e+04
#3	5.238e-02	2295	1.539e+05
#4	3.822e-02	4255	3.416e+05
#5	3.009e-02	6815	6.246e+05
#6	2.481e-02	9975	1.015e+06
#7	2.111e-02	13735	1.525e+06
#8	1.837e-02	18095	2.163e+06
#9	1.626e-02	23055	2.939e+06
#10	1.458e-02	28615	3.862e+06

TABLE 1. Characteristics of the family of structured meshes used in the simulations: size  $h$ , number of degrees of freedom (*d.o.f.*) and condition number ( $\text{cond}_2(\mathbb{A})$ ) of the XFEM-edge elements matrix.

A well-known issue in the implementation of XFEM is the need of accurate evaluation of the coefficients in the matrix of the linear system corresponding to the enriched degrees of freedom since the corresponding basis functions contain discontinuities and/or singularities (see e.g. [20, 26]). In our concerns, we have to pay special attention to the computation of the matrix  $\mathbb{A}_{ee'}^{\mathcal{E}\mathcal{E}H}$  and the vector  $C$ . Notice that the coefficient  $a_s$  can be evaluated analytically since it reduces to the integral of a polynomial function in  $r$  and a trigonometric function in  $\theta$  provided the cut-off function  $\eta_1 = \eta_1(r)$  is a polynomial in the local variable  $r$ ,

$$\begin{aligned} a_s &= a(\text{grad}(\eta_1 S_1), \text{grad}(\eta_1 S_1)) \\ &= -\kappa^2 \varepsilon_r \int_{\Omega} |\text{grad}(\eta_1 S_1)|^2 d\mathbf{x} \\ &= -\kappa^2 \varepsilon_r \int_0^b \int_{-\pi}^{\pi} \left( |\partial_r(\eta_1(r) S_1(r, \theta))|^2 + \left| \frac{1}{r} \partial_{\theta}(\eta_1(r) S_1(r, \theta)) \right|^2 \right) r d\theta dr \\ &= -\kappa^2 \varepsilon_r \int_0^b \int_{-\pi}^{\pi} \left( (|\eta_1'(r)|^2 r^2 + \eta_1'(r) \eta_1(r) r) \sin^2 \frac{\theta}{2} + \frac{1}{4} |\eta_1(r)|^2 \right) d\theta dr. \end{aligned}$$

In the numerical tests,  $\eta_1$  is given by the following piecewise polynomial function of class  $\mathcal{C}^2$ ,

$$\eta_1(r) = \begin{cases} 1 & \text{if } 0 \leq r < a \\ p_{\eta}(r) & \text{if } a \leq r < b \\ 0 & \text{if } r \geq b. \end{cases}$$

where  $p_{\eta}$  is a polynomial of degree 5 in  $r$  in order to satisfy the regularity assumptions on  $\eta_1$ .

The coefficients of the matrix  $\mathbb{A}_{ee'}^{\mathcal{E}\mathcal{E}H}$  are computed *via* a partition of the enriched triangles into 3 subtriangles conforming to the crack geometry (see Figure 4, left). On each subtriangle, we use 7 Gauss points leading to a quadrature rule of order 5 (Stroud-Hadamard formula). Notice that even if the subdivision leads to triangles with small angles, this does not affect the quality of the mesh since it is only used to perform numerical integration. The coefficients of the vector  $C$  are computed using the Stroud-Hadamard formula for any triangle that does not contain the crack tip. The crack tip triangle is divided into four subtriangles having the crack tip as vertex (see Figure 4, right).

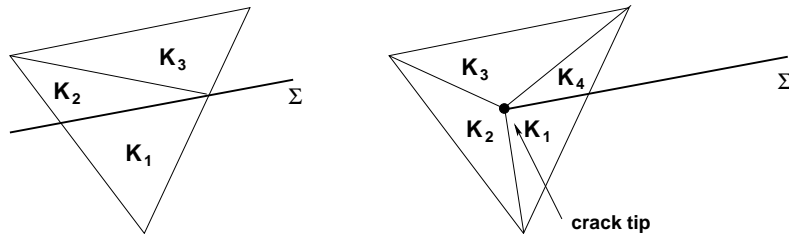


FIGURE 4. Subdivision of the enriched (left) and crack tip (right) triangles

On each subtriangle, we use a quasi-polar quadrature rule as in [20]. This quadrature rule is obtained from a classical Gauss formula on the unit square using the transformation

$$\tau : \begin{cases} [0, 1] \times [0, 1] & \rightarrow \hat{K} \\ (x_1, x_2) & \mapsto (x_1 x_2, x_2) \end{cases}$$

where  $\hat{K}$  is the triangle of vertices  $(0, 0)$ ,  $(1, 1)$  and  $(0, 1)$  and  $(0, 0)$  is mapped to the crack tip (see Figure 5). This allows for using quadrature rules of arbitrary order derived from Gauss formula on the interval  $[0, 1]$ . Actually, we used 5 points in each direction.

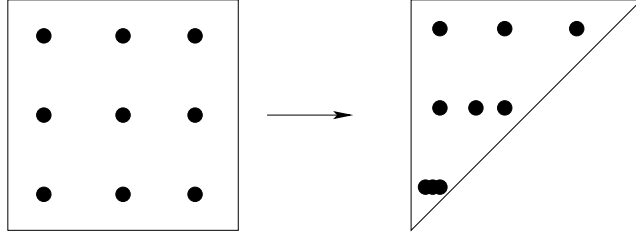


FIGURE 5. Quadrature points for the quasi-polar formula

In order to perform error analysis, one has to evaluate the norms in an accurate way. Usually, this is done by computing a simple vector-matrix-vector product

$$|(U_{\text{ex}} - U)^* \mathbb{A} (U_{\text{ex}} - U)|^{1/2}$$

which is actually the error between the interpolate of the exact solution and the computed numerical solution in the norm induced by the matrix  $\mathbb{A}$ . In the case of the XFEM method, the evaluation is somewhat tricky since the interpolate of the exact solution depends on the extension operator and thus can not be easily computed. We thus proceed by numerical integration. Let  $\mathbf{u}$  be the exact solution. The numerical solution  $\mathbf{u}_h$  splits in the following way in a purely finite element part  $\mathbf{u}_{r,h}$  (the "regular" part) and a singular part,

$$\mathbf{u}_h = \mathbf{u}_{r,h} + u_s \text{grad}(\eta_1 S_1)$$

with

$$\mathbf{u}_{r,h} \in \text{Vect}(\mathbf{w}_e | e \in \mathcal{E}) \oplus \text{Vect}(H\mathbf{w}_e | e \in \mathcal{E}_H).$$

Developping the  $L^2$ -norm of the error yields,

$$\begin{aligned} \|\mathbf{u} - \mathbf{u}_h\|_{0,\Omega}^2 &= \|\mathbf{u} - \mathbf{u}_{r,h} - u_s \text{grad}(\eta_1 S_1)\|_{0,\Omega}^2 \\ &= \|\mathbf{u}\|_{0,\Omega}^2 - 2 \Re e(\mathbf{u}, \mathbf{u}_{r,h}) + \|\mathbf{u}_{r,h}\|_{0,\Omega}^2 \\ &\quad - 2 \Re e(\mathbf{u}, u_s \text{grad}(\eta_1 S_1)) + 2 \Re e(\mathbf{u}_{r,h}, u_s \text{grad}(\eta_1 S_1)) \\ &\quad + |u_s|^2 \|\text{grad}(\eta_1 S_1)\|_{0,\Omega}^2. \end{aligned}$$

Now, the term

$$\|\mathbf{u}\|_{0,\Omega}^2 - 2 \Re e(\mathbf{u}, u_s \text{grad}(\eta_1 S_1)) + |u_s|^2 \|\text{grad}(\eta_1 S_1)\|_{0,\Omega}^2$$

can be computed *via* numerical integration independantly of the mesh. The term  $(\mathbf{u}, \mathbf{u}_{r,h})$  can be decomposed onto the basis functions of finite element type ( $\mathbf{w}_e$  and  $H\mathbf{w}_e$ ) and we have

$$(\mathbf{u}, \mathbf{u}_{r,h}) = U_r^* W$$

where the vector  $W$  is given by

$$W_e = \begin{cases} (\mathbf{u}, \mathbf{w}_e) & \text{if } e \in \mathcal{E} \\ (\mathbf{u}, H\mathbf{w}_e) & \text{if } e \in \mathcal{E}_H \end{cases}$$

which is of the same nature as the right hand side  $F$ . In the same way, we have

$$(\mathbf{u}_{r,h}, u_s \text{grad}(\eta_1 S_1)) = \overline{u_s} G^* U_r$$

where the (real-valued) coefficients of the vector  $G$  are defined by

$$G_e = \begin{cases} (\mathbf{w}_e, \text{grad}(\eta_1 S_1)) & \text{if } e \in \mathcal{E} \\ (H\mathbf{w}_e, \text{grad}(\eta_1 S_1)) & \text{if } e \in \mathcal{E}_H \end{cases} .$$

Notice that  $G$  is related to the vector  $C$  by  $C = -\kappa^2 \epsilon_r G$ . Finally, we have

$$\|\mathbf{u}_{r,h}\|_{0,\Omega}^2 = U_r^* \mathbb{M} U_r$$

where  $\mathbb{M}$  denotes the mass matrix corresponding to the basis functions  $(\mathbf{w}_e)_{e \in \mathcal{E}}$  and  $(H\mathbf{w}_e)_{e \in \mathcal{E}_H}$ . The semi-norm  $\|\text{curl}(\mathbf{u} - \mathbf{u}_h)\|_{0,\Omega}$  of the error can be computed in a similar way. We actually have

$$\|\text{curl}(\mathbf{u} - \mathbf{u}_h)\|_{0,\Omega}^2 = \|\text{curl} \mathbf{u}\|_{0,\Omega}^2 - 2 \Re e(\text{curl} \mathbf{u}, \text{curl} \mathbf{u}_{r,h}) + \|\text{curl} \mathbf{u}_{r,h}\|_{0,\Omega}^2 .$$

Again,  $\|\text{curl} \mathbf{u}\|_{0,\Omega}^2$  can be computed independently of the mesh and  $(\text{curl} \mathbf{u}, \text{curl} \mathbf{u}_{r,h})$  reads as

$$(\text{curl} \mathbf{u}, \text{curl} \mathbf{u}_{r,h}) = U_r^* R$$

where the vector  $R$  is given by

$$R_e = \begin{cases} (\text{curl} \mathbf{u}, \text{curl} \mathbf{w}_e) & \text{if } e \in \mathcal{E} \\ (\text{curl} \mathbf{u}, \text{curl}(H\mathbf{w}_e)) & \text{if } e \in \mathcal{E}_H . \end{cases}$$

Finally, we have  $\|\text{curl} \mathbf{u}_{r,h}\|_{0,\Omega}^2 = U_r^* \mathbb{K} U_r$  where the symmetric matrix  $\mathbb{K}$  is defined by

$$\mathbb{K}_{ee'} = \begin{cases} (\text{curl} \mathbf{w}_{e'}, \text{curl} \mathbf{w}_e) & \text{if } e, e' \in \mathcal{E} \\ (\text{curl} \mathbf{w}_{e'}, \text{curl}(H\mathbf{w}_e)) & \text{if } e \in \mathcal{E}_H \text{ and } e' \in \mathcal{E} \\ (\text{curl}(H\mathbf{w}_{e'}), \text{curl}(H\mathbf{w}_e)) & \text{if } e \in \mathcal{E}_H . \end{cases}$$

We have tested our method with the following exact solutions.

In the first example, named *polynomial solution*, the exact solution is piecewise polynomial in  $\Omega$ ,

$$(27) \quad \mathbf{u}(x, y) = \begin{cases} \begin{pmatrix} x^2 \\ xy^2 \end{pmatrix} & \text{if } x < 0 \\ \begin{pmatrix} \text{sign}(y)x^2 \\ xy^2 \end{pmatrix} & \text{if } x \geq 0 . \end{cases}$$

Notice that  $\mathbf{u}$  belongs to  $H^2(\Omega)^2$ . The tangential component of  $\mathbf{u}$  is discontinuous across the crack  $\Sigma$ , whereas the normal component is vanishing. Hence,  $\text{div} \mathbf{u} \in L^2(Q)$ .

In the second example, the exact solution is singular near the crack tip and does present a discontinuity across the crack (see Figure 6),

$$(28) \quad \mathbf{u}(r, \theta) = \text{grad} \left( r^{1/2} \sin \frac{\theta}{2} \right) ,$$

where  $(r, \theta)$  are the local polar coordinates with respect to the crack tip. Notice that  $\mathbf{u}$  coincides with the singular field near the crack tip, but is not contained in the discretization space.

In the third example, the singular part of the exact solution vanishes, but the regular part only belongs to  $H^{3/2-\eta}(\Omega)^2$ . Below, this solution is referred to as a *hybrid solution* and is plotted in Figure 7. It is derived from the second singular function of the corresponding scalar Laplace equation and reads as follows in local polar coordinates,

$$(29) \quad \mathbf{u}(r, \theta) = \text{grad} \left( r^{3/2} \sin \frac{3\theta}{2} \right) .$$

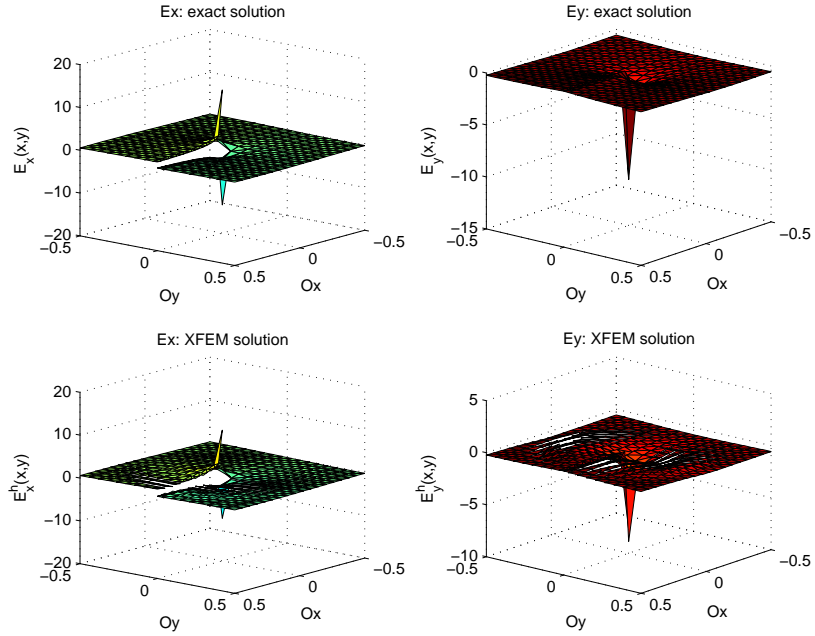


FIGURE 6. The exact singular solution  $(E_x, E_y)$  (top) and its XFEM-edge approximation (bottom).

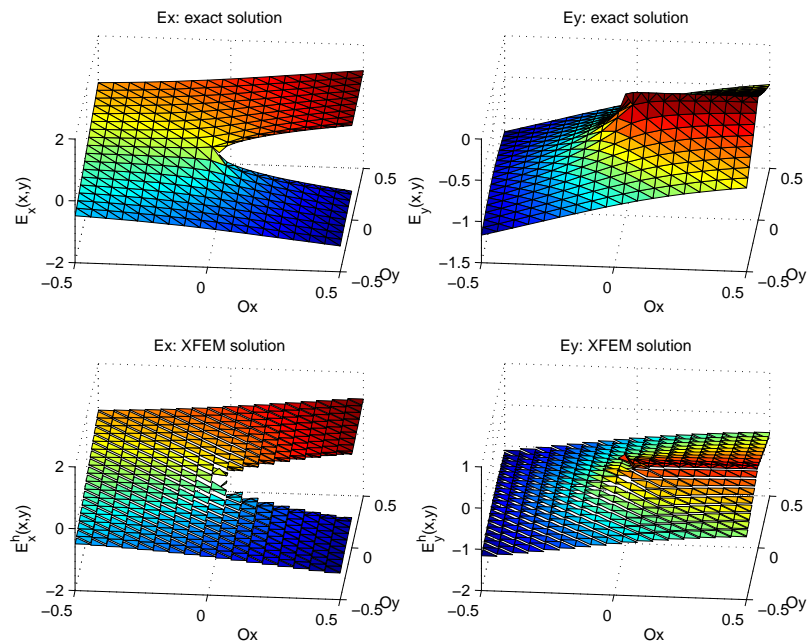


FIGURE 7. The exact hybrid solution  $(E_x, E_y)$  (top) and its XFEM-edge approximation (bottom).

Whereas the second and third example deal with gradients, the exact solution in the last example is not curl free. The analytic expression of the solution is derived from the third term in the asymptotic expansion in singular terms following [11], and is given in local coordinates by

$$(30) \quad \mathbf{u}(r, \theta) = r^{3/2} \cos\left(\frac{3\theta}{2}\right) \mathbf{n}_\Sigma + r^{3/2} \sin\left(\frac{3\theta}{2}\right) \boldsymbol{\tau}_\Sigma.$$

Notice that  $\mathbf{u}$  belongs to  $H^2(\Omega)^2$  and we thus refer to it as a *regular solution*.

In all numerical tests, the values of the parameters have been fixed to  $\mu_r = 1$ ,  $\varepsilon_r = 1 + i$  and  $\kappa = 1$ . The crack tip  $x^*$  is located at  $(-\delta, 0)$  with  $\delta = 2.10^{-4}$ .

mesh	$\ \text{curl}(e_h)\ _{0,\Omega}$	$\tau$	$\ e_h\ _{0,\Omega}$	$\tau$	$u_s$
#1	1.976e-02	–	2.560e-02	–	-3.3e-03 -6.6e-05i
#2	8.080e-03	1.0079	1.064e-02	0.9893	-1.4e-03 -2.4e-06i
#3	5.072e-03	1.0066	6.708e-03	0.9972	-9.1e-04 +4.4e-07i
#4	3.695e-03	1.0050	4.897e-03	0.9987	-6.9e-04 +6.4e-07i
#5	2.906e-03	1.0039	3.856e-03	0.9992	-5.6e-04 +4.4e-07i
#6	2.395e-03	1.0033	3.180e-03	0.9995	-4.7e-04 +2.1e-07i
#7	2.037e-03	1.0028	2.705e-03	0.9996	-4.0e-04 -1.0e-08i
#8	1.771e-03	1.0024	2.354e-03	0.9996	-3.5e-04 -1.9e-07i
#9	1.567e-03	1.0022	2.084e-03	0.9998	-3.1e-04 -3.5e-07i
#10	1.406e-03	1.0019	1.869e-03	0.9997	-2.8e-04 -4.9e-07i

TABLE 2. Errors, numerical convergence rates ( $\tau$ ), and singular coefficients ( $u_s$ ) for the polynomial solution (27).

mesh	$\ \text{curl}(e_h)\ _{0,\Omega}$	$\tau$	$\ e_h\ _{0,\Omega}$	$\tau$	$u_s$
#1	8.893e-02	–	2.511e-01	–	5.8e-01 +2.6e-02i
#2	1.998e-02	1.6826	1.191e-01	0.8411	7.2e-01 +7.3e-03i
#3	8.955e-03	1.7352	7.955e-02	0.8718	8.0e-01 +3.6e-03i
#4	5.114e-03	1.7781	5.986e-02	0.9026	8.4e-01 +2.1e-03i
#5	3.324e-03	1.8004	4.802e-02	0.9217	8.7e-01 +1.4e-03i
#6	2.343e-03	1.8125	4.009e-02	0.9349	8.9e-01 +1.0e-03i
#7	1.747e-03	1.8176	3.442e-02	0.9437	9.1e-01 +7.6e-04i
#8	1.356e-03	1.8203	3.016e-02	0.9511	9.2e-01 +5.9e-04i
#9	1.086e-03	1.8203	2.683e-02	0.9566	9.3e-01 +4.7e-04i
#10	8.908e-04	1.8188	2.417e-02	0.9611	9.3e-01 +3.9e-04i

TABLE 3. Errors, numerical convergence rates ( $\tau$ ), and singular coefficients ( $u_s$ ) for the singular solution (28).

Tables 2–5 show the numerical convergence rates of the error  $\mathbf{e}_h = \mathbf{u} - \mathbf{u}_h$  in the semi-norm of  $\mathcal{H}(\text{curl}; \Omega)$  and the  $L^2$ -norm.

For the polynomial solution (table 2), we get optimal error estimates in both the semi-norm and the  $L^2$ -norm which validates the code. In the case of the singular solution, the convergence rate in the  $L^2$ -norm seems to converge to 1 (see table 3). This is in concordance with the error analysis performed in §4. Indeed, the singular solution may be written as

$$\mathbf{u} = \text{grad}((1 - \eta_1)S_1) + \text{grad}(\eta_1 S_1),$$

mesh	$\ \text{curl}(e_h)\ _{0,\Omega}$	$\tau$	$\ e_h\ _{0,\Omega}$	$\tau$	$u_s$
#1	4.121e-02	–	1.014e-01	–	-3.9e-02 -2.0e-03i
#2	1.081e-02	1.5081	4.128e-02	1.0135	-2.1e-02 -2.4e-04i
#3	5.399e-03	1.5010	2.598e-02	1.0010	-1.5e-02 -7.4e-05i
#4	3.365e-03	1.5002	1.896e-02	0.9991	-1.2e-02 -3.2e-05i
#5	2.350e-03	1.5000	1.493e-02	0.9985	-9.8e-03 -1.6e-05i
#6	1.760e-03	1.5000	1.232e-02	0.9985	-8.3e-03 -9.8e-06i
#7	1.381e-03	1.4999	1.048e-02	0.9984	-7.2e-03 -6.2e-06i
#8	1.121e-03	1.5000	9.124e-03	0.9984	-6.3e-03 -4.2e-06i
#9	9.334e-04	1.4998	8.077e-03	0.9986	-5.7e-03 -2.9e-06i
#10	7.929e-04	1.5000	7.245e-03	0.9985	-5.1e-03 -2.1e-06i

TABLE 4. Errors, numerical convergence rates ( $\tau$ ), and singular coefficients ( $u_s$ ) for the hybrid solution (29).

mesh	$\ \text{curl}(e_h)\ _{0,\Omega}$	$\tau$	$\ e_h\ _{0,\Omega}$	$\tau$	$u_s$
#1	9.019e-02	–	3.901e-02	–	1.4e-02 -1.1e-02i
#2	3.806e-02	0.9725	1.706e-02	0.9320	1.4e-02 -1.3e-02i
#3	2.415e-02	0.9828	1.133e-02	0.8851	1.5e-02 -1.4e-02i
#4	1.770e-02	0.9872	8.667e-03	0.8500	1.5e-02 -1.5e-02i
#5	1.397e-02	0.9897	7.113e-03	0.8265	1.5e-02 -1.5e-02i
#6	1.153e-02	0.9914	6.079e-03	0.8136	1.6e-02 -1.6e-02i
#7	9.825e-03	0.9925	5.333e-03	0.8102	1.6e-02 -1.6e-02i
#8	8.557e-03	0.9933	4.761e-03	0.8153	1.5e-02 -1.5e-02i
#9	7.579e-03	0.9941	4.304e-03	0.8281	1.5e-02 -1.5e-02i
#10	6.801e-03	0.9945	3.925e-03	0.8473	1.5e-02 -1.5e-02i

TABLE 5. Errors, numerical convergence rates ( $\tau$ ), and singular coefficients ( $u_s$ ) for the regular solution (30).

and the regular part  $\mathbf{u}_r = \text{grad}((1 - \eta_1)S_1)$  belongs to  $H^2(\Omega)^2$ . The theoretical convergence rate is thus equal to 1.

For the hybrid solution, the error estimate (16) in §4 yields a convergence rate of 0.5. This is lower than the observed numerical rate which is almost 1 in the  $L^2$ -norm and even 1.5 in the semi-norm of  $\mathcal{H}(\text{curl}; \Omega)$  (see table 4). Maybe this is due to the choice of the specific example of the hybrid solution which is a gradient. On the other hand, it is worthwhile noticing that the local interpolation error estimates (18) and (19) in §4 yield a convergence to zero as  $\mathcal{O}(h)$  on all triangles except the crack tip triangle and one neighboring element (where it is as  $\mathcal{O}(h^{1/2-\eta})$ ) since  $\mathbf{u} \in \mathcal{H}^1(\text{curl}; \Omega)$ .

Finally, in the case of the regular solution which is not curl free, we get a numerical convergence rate about 1 in the semi-norm and 0.85 in the  $L^2$ -norm (see table 5). We also observe that the convergence of the singular coefficient is more hesitant than in the other examples. A similar behaviour in the case of solutions which are not gradients has been mentioned in [19] in the context of the *Singular Field Method* which is based on geometry-fitting Lagrange Finite Elements.

In Figure 8, we compare our new XFEM-edge method with a classical method using first order edge elements on a geometry-fitting mesh. We represent the error

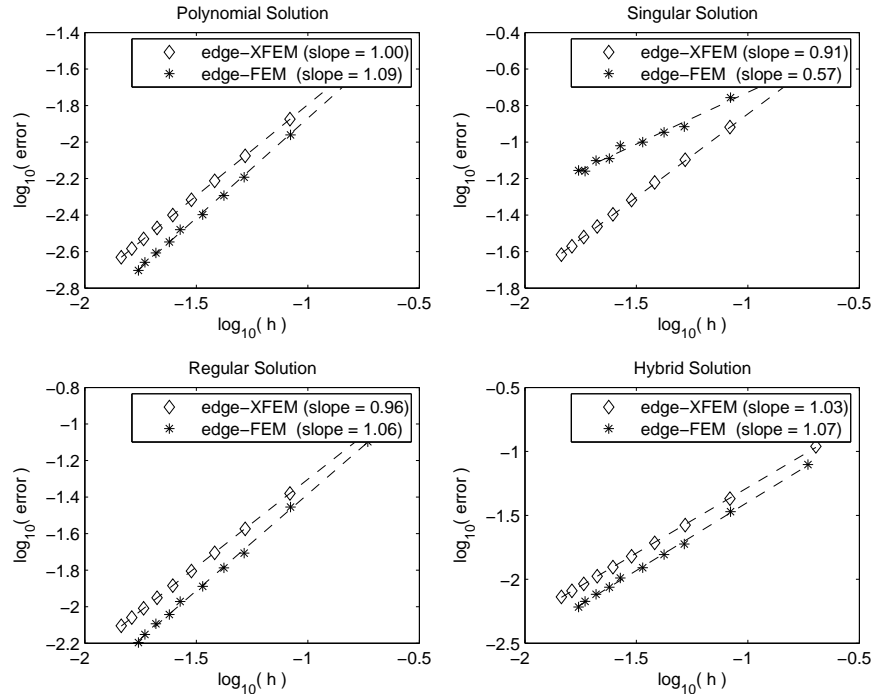


FIGURE 8. Comparison of classical and eXtended edge elements.

in the full  $\mathcal{H}(\text{curl}; \Omega)$ -norm. In the case of the polynomial solution, both methods converge with the optimal rate 1 and the errors are nearly the same. For the singular solution, the performance of the new XFEM-edge method is much better than the classical one: we get a slope of 0.91 for XFEM compared to 0.57. In the case of the hybrid and the regular solution, classical edge elements seem to perform a little better than XFEM, but the difference in the errors is rather small and the numerical convergence rates are nearly the same.

## 6. Conclusion

We proposed a new eXtended Finite Element Method based on two dimensional edge elements to solve the time-harmonic Maxwell equations in a cracked domain. The standard finite element space has been enriched on the one hand with basis functions of Heaviside type in order to allow the tangential component of the electric field to be discontinuous across the crack, and with a singular field localized at the crack tip on the other in order to take into account the singular behavior of the solution field. The error analysis yields a convergence rate of at least  $1/2$ , depending on the regularity of the regular part of the exact solution. Notice however, that the interpolation error converges to zero with optimal rate on all triangles except the crack tip triangle and one neighboring element. The numerical results show that our XFEM-edge method is able to simulate discontinuities and singular behavior of the electric field on a mesh that is independent from the crack location. It performs better than classical edge elements in the physically relevant situation where the electric field presents a singularity, and yields comparable results for regular fields.

In order to overcome the influence of the cut-off function and its well-known "pollution effect", variants of the actual XFEM-edge method could be implemented. In

[7], an eXtended Finite Element Method based on Lagrange Finite Elements with integral matching has been tested in the context of linear elasticity. In electromagnetics, the *Singular Complement Method* (see [2]) and the *Orthogonal Singular Field Method* (see [19]) based on geometry-fitting Lagrange Finite Elements on non-convex polygons are examples how to deal with the singularities of the electromagnetic field without making use of a cut-off function.

### Appendix A. Properties of the scalar and vector extension operator

In this section, we define the extension operators  $\mathbf{E}^\pm$  involved in the error analysis of §3.

Without restriction of generality, we assume here that the straight line  $\mathcal{D}$  does coincide with the  $x_1$ -axis and that  $\Omega^+$  is the upper half plane. Indeed, with the help of a partition of unity we localize the problem to a neighborhood of  $\mathcal{D} \cap \overline{Q}$  and a linear change of variables (rotation) maps  $\mathcal{D}$  onto the  $x_1$ -axis. These transformations do not affect the involved norms. We will give details of the definition and the properties only for the operator  $\mathbf{E}^+$  which extends fields from  $\Omega^+$  to  $\Omega^-$ . All results keep true in an analogous manner for the extension  $\mathbf{E}^-$  from  $\Omega^-$  to  $\Omega^+$ .

Let  $\lambda_j$ ,  $1 \leq j \leq 3$ , be such that

$$(31) \quad \sum_{j=1}^3 (-j)^k \lambda_j = 1 \quad \forall 0 \leq k \leq 2.$$

The scalar extension operator  $E^+$  is defined as follows. Let  $p$  be a smooth function defined on  $\Omega^+$ . Then

$$(32) \quad E^+ p(x_1, x_2) = \begin{cases} p(x_1, x_2) & \text{if } x_2 > 0 \\ \sum_{j=1}^3 \lambda_j p(x_1, -jx_2) & \text{if } x_2 < 0. \end{cases}$$

The following result is classical (see e.g. [1, 16]).

**Proposition 4.** *Let  $s \in [0, 2]$  and let  $p$  be a smooth function defined on  $\overline{\Omega^+}$ . Then  $E^+ p \in H^s(\mathbb{R}^2)$  and there is a constant  $C > 0$  independent from  $p$  such that*

$$\|E^+ p\|_{s, \mathbb{R}^2} \leq C \|p\|_{s, \Omega^+}$$

for any smooth function  $p$  defined on  $\overline{\Omega^+}$ .

By density, the operator  $E^+$  admits an extension which is a linear continuous application from  $H^s(\Omega^+)$  into  $H^s(\mathbb{R}^2)$ .

We now aim to define an extension operator  $\mathbf{E}^+$  for vector fields. Let  $\mathbf{v} = (v_1, v_2)^t \in C^\infty(\overline{\Omega^+})^2$ . Then the vector field  $\mathbf{E}^+ \mathbf{v}$  is defined by

$$(33) \quad \mathbf{E}^+ \mathbf{v}(x_1, x_2) = \begin{cases} \mathbf{v}(x_1, x_2) & \text{if } x_2 > 0 \\ \sum_{j=1}^3 \lambda_j (v_1(x_1, -jx_2) \mathbf{e}_1 - jv_2(x_1, -jx_2) \mathbf{e}_2) & \text{if } x_2 < 0. \end{cases}$$

The following result follows from Proposition 4 and the definition of the parameters  $\lambda_j$ .

**Proposition 5.** *Let  $s \in [0, 2]$  and let  $\mathbf{v}$  be a smooth vector field defined on  $\overline{\Omega^+}$ . Then  $\mathbf{E}^+ \mathbf{v} \in H^s(\mathbb{R}^2)^2$  and there is a constant  $C > 0$  independent from  $\mathbf{v}$  such that*

$$\|\mathbf{E}^+ \mathbf{v}\|_{s, \mathbb{R}^2} \leq C \|\mathbf{v}\|_{s, \Omega^+}.$$

It follows from classical density results that the operator  $\mathbf{E}^+$  admits an extension which is a linear continuous application from  $H^s(\Omega^+)^2$  into  $H^s(\mathbb{R}^2)^2$ .

Now, let

$$\mathcal{H}^s(\text{curl}; \Omega) = \{ \mathbf{u} \in H^s(\Omega)^2 \mid \text{curl } \mathbf{u} \in H^s(\Omega) \}$$

where  $s \geq 0$ . The extension operator  $\mathbf{E}^+$  conserve regularity of the curl in the following way.

**Proposition 6.** *For all  $s \in [0, 1]$ , the extension operator  $\mathbf{E}^+$  defines a linear continuous application from  $\mathcal{H}^s(\text{curl}; \Omega^+)$  into  $\mathcal{H}^s(\text{curl}; \mathbb{R}^2)$ .*

*Proof.* Let  $\mathbf{v} \in \mathcal{C}^\infty(\overline{\Omega^+})^2$ . For  $x_2 < 0$ , we have

$$\begin{aligned} \text{curl}(\mathbf{E}^+ \mathbf{v})(x_1, x_2) &= \frac{\partial(\mathbf{E}^+ \mathbf{v})_2}{\partial x_1}(x_1, x_2) - \frac{\partial(\mathbf{E}^+ \mathbf{v})_1}{\partial x_2}(x_1, x_2) \\ &= \sum_{j=1}^3 -j\lambda_j \frac{\partial v_2}{\partial x_1}(x_1, -jx_2) + j\lambda_j \frac{\partial v_1}{\partial x_2}(x_1, -jx_2) \\ &= \sum_{j=1}^3 -j\lambda_j (\text{curl } \mathbf{v})(x_1, -jx_2). \end{aligned}$$

Hence,  $\text{curl}(\mathbf{E}^+ \mathbf{v})|_{\Omega^-}$  has the same regularity as  $\text{curl } \mathbf{v}$ . We further have

$$\text{curl}(\mathbf{E}^+ \mathbf{v})|_{\Omega^-}(x_1, 0) = \sum_{j=1}^3 -j\lambda_j \text{curl } \mathbf{v}(x_1, 0) = \text{curl } \mathbf{v}(x_1, 0)$$

since  $\sum_{j=1}^3 (-j\lambda_j) = 1$ . This proves that the extension of the curl is continuous across  $\mathcal{D}$ . Hence,  $\text{curl } \mathbf{E}^+ \mathbf{v} \in H^1(\mathbb{R}^2)$  and

$$\| \mathbf{E}^+ \mathbf{v} \|_{\mathcal{H}^1(\text{curl}; \mathbb{R}^2)} \lesssim \| \mathbf{v} \|_{\mathcal{H}^1(\text{curl}; \Omega^+)}.$$

These results keep true for  $\mathbf{v} \in \mathcal{H}(\text{curl}; \Omega^+)$  and  $\mathbf{v} \in \mathcal{H}^1(\text{curl}; \Omega^+)$  by density. For  $0 < s < 1$ , the result then follows from interpolation theory.  $\square$

## References

- [1] R. A. Adams and J. Fournier, Sobolev Spaces, Academic Press, Oxford, 2003
- [2] F. Assous, P. Ciarlet Jr., and J. Segré, Numerical solution to the time-dependent Maxwell equations in two-dimensional domains: the singular complement method, *J. Comput. Phys.*, 161 (2000), pp. 218–249.
- [3] E. Béchet, H. Minnebo, N. Moës, and B. Burgardt, Improved implementation and robustness study of the X-FEM for stress analysis around cracks, *Int. J. Numer. Meth. Engng.*, 64 (2005), pp. 1033–1056.
- [4] A.-S. Bonnet-Ben Dhia, C. Hazard C., and S. Lohrengel, A singular field method for the solution of Maxwell's equations in polyhedral domains., *SIAM J. Appl. Math.*, 59 (1999), pp. 2028–2044.
- [5] V. A. Bokil and R. Glowinski, An operator splitting scheme with a distributed Lagrange multiplier based fictitious domain method for wave propagation problems, *J. Comput. Phys.*, 205 (2005), pp. 242–268.
- [6] E. Chahine, P. Laborde, and Y. Renard, Crack-tip enrichment in the XFEM method using a cut-off function, *Int. J. Numer. Meth. Engng.*, 75 (2008), pp. 629–646.
- [7] E. Chahine, P. Laborde, and Y. Renard., A non-conformal eXtended Finite Element approach: Integral matching Xfem, *Appl. Numer. Math.*, 61 (2011), pp. 322–343.
- [8] E. Chahine, S. Nicaise, and Y. Renard, Optimal convergence analysis for the extended finite element method, *Int. J. Numer. Meth. Engng.*, 86 (2011), pp. 528–548.
- [9] J. Chessa and T. Belytschko, An extended finite element method for two-phase fluids, *ASME J. Appl. Mech.*, 70 (2003), pp. 10–17.
- [10] P.C. Ciarlet, The Finite Element Method for Elliptic Problems, Volume 4 of *Studies In Mathematics and Its Applications*, North-Holland, New York, 1978.

- [11] M. Costabel and M. Dauge, Singularities of electromagnetic fields in polyhedral domains, *Arch. Rational Mech. Anal.*, 151 (2000), pp. 221–276.
- [12] F. Collino, P. Joly, and F. Millot, Fictitious Domain Method for Unsteady Problems: Application to Electromagnetic Scattering, *J. Comput. Phys.*, 138 (1997), pp. 907–938.
- [13] W. Dahmen, T. Klint, and K. Urban, On Fictitious Domain Formulations for Maxwell's Equations, *Foundations of Computational Mathematics*, 3 (2003), pp. 135–143.
- [14] A. Gerstenberger, and W. A. Wall, An eXtended finite element method/Lagrange multiplier based approach for fluid-structure interaction, *Comp. Methods Appl. Mech. Engrg.*, 197 (2008), pp. 1699-1714.
- [15] A. Gravouil, N. Moës, and T. Belytschko, Non-planar 3D crack growth by the extended finite element method and level sets, Part II: Level set update, *Int. J. Numer. Meth. Engrg.*, 53 (2002), pp. 2569-2586.
- [16] P. Grisvard, *Singularities in boundary value problems*, Masson, Paris, 1992.
- [17] J. Haslinger and Y. Renard, A new fictitious domain method inspired by the extended finite element method, *SIAM J. Numer. Anal.*, 47 (2009), pp. 1474–1499.
- [18] C. Hazard and M. Lenoir, On the Solution of Time-Harmonic Scattering Problems for Maxwell's Equations, *SIAM J. Math. Anal.*, 27 (1996), pp. 1597–1630.
- [19] C. Hazard and S. Lohrengel, A singular field method for Maxwell's equations: numerical aspects for 2D magnetostatics. *SIAM J. Numer. Anal.*, 40 (2002), pp. 1021–1040.
- [20] P. Laborde, Y. Renard, J. Pommier, and M. Salaün, High Order Extended Finite Element Method For Cracked Domains, *Int. J. Numer. Meth. Engrg.*, 64 (2005), pp. 354–381.
- [21] S. Lohrengel, *Etude mathématique et résolution numérique des équations de Maxwell dans un domaine non régulier*, Thesis (in french), University of Paris 6, Paris, France, 1998.
- [22] N. Moës, E. Béchet, and M. Tourbier, Imposing Dirichlet boundary conditions in the eXtended Finite Element Method, *Int. J. Numer. Meth. Engrg.*, 12 (2006), pp. 354381.
- [23] N. Moës, J. Dolbow, J., and T. Belytschko, A finite element method for crack growth without remeshing, *Int. J. Numer. Meth. Engrg.*, 46 (1999), pp. 131–150.
- [24] N. Moës, A. Gravouil, and T. Belytschko, Non-planar 3D crack growth by the extended finite element method and level sets, Part I: Mechanical model, *Int. J. Numer. Meth. Engrg.*, 53 (2002), pp. 2549-2568.
- [25] P. Monk, *Finite Element Methods for Maxwell's Equations*, Oxford University Press, 2003.
- [26] S. E. Mousavi, H. Xiao, and N. Sukumar, Generalized Gaussian quadrature rules on arbitrary polygons, submitted.
- [27] M. Moussaoui, *Espaces  $H(\text{div}, \text{rot}, \Omega)$  dans un polygone plan*, *C. R. Acad. Sc. Paris, Série I*, 322 (1996), pp. 225–229.
- [28] J. C. Nédélec, Mixed finite elements in  $\mathbb{R}^3$ , *Numer. Math.*, 35 (1980), pp. 315–341.
- [29] S. Nicaise, Edge elements on anisotropic meshes and approximation of the Maxwell equations, *SIAM J. Numer. Anal.*, 39 (2001), pp. 784–816.
- [30] G. Strang, and G. Fix, *An Analysis of the Finite Element Method*, Prentice-Hall, Englewood Cliffs, 1973.
- [31] N. Sukumar, D. L. Chopp, N. Moës, and T. Belytschko Modeling holes and inclusions by level sets in the extended finite element method, *Comput. Methods Appl. Mech. Eng.*, 46 (2001), pp. 61836200.
- [32] N. Sukumar, N. Moës, B. Moran, and T. Belytschko, Extended finite element method for three dimensional crack modelling, *Int. J. Numer. Meth. Engrg.*, 48 (2000), pp. 1549–1570.

Laboratoire de Mathématiques, Université de Reims Champagne-Ardenne, Moulin de la Housse  
- B.P. 1039, 51687 Reims Cedex 2, France

*E-mail:* francois.lefevre@univ-reims.fr and stephanie.lohrengel@univ-reims.fr

LAMAV, Université de Valenciennes et du Hainaut Cambrésis, Le Mont Houy, 59313 Valenciennes Cedex 9, France

*E-mail:* serge.nicaise@univ-valenciennes.fr